8-2011

Surface Symmetry Energy of Nuclear Energy Density Functionals

Nikola Iliev Nikolov
nnikolov@utk.edu

To the Graduate Council:

I am submitting herewith a dissertation written by Nikola Iliev Nikolov entitled "Surface Symmetry Energy of Nuclear Energy Density Functionals." I have examined the final electronic copy of this dissertation for form and content and recommend that it be accepted in partial fulfillment of the requirements for the degree of Doctor of Philosophy, with a major in Physics.

Witold Nazarewicz, Major Professor

We have read this dissertation and recommend its acceptance:

Lawrence W. Townsend, Thomas Papenbrock, Robert Grzywacz

Accepted for the Council:

Carolyn R. Hodges

Vice Provost and Dean of the Graduate School

(Original signatures are on file with official student records.)

Surface Symmetry Energy of Nuclear Energy Density Functionals

A Dissertation
Presented for the
Doctor of Philosophy Degree
The University Of Tennessee, Knoxville

Nikola Iliev Nikolov
Augus 2011

Acknowledgments

The current research has been performed with the help and critics of others. First, I would like to thank my academic advisor, Prof. Witold Nazarewicz, for his support. He gave me the opportunity to work on two excellent research projects during my PhD. Both of these projects finished with published peer-review articles. This could not happen without hard work, scientific critics, and patience, which I learned from my academic advisor, and I am going to use in future.

I would like to thank Dr. Nicolas Schunck, for all of the times of discussions and all his developments on HFODD, which I used in my research. HFODD is one of the most sophisticated Hartree-Fock-Bogoliubov codes in nuclear structure ($\sim$ 116 000 lines). Without the help from Nicolas Schunck, I could not understand HFODD in details, and I could not complete my research and thesis.

I would like to thank Dr. Mario Stoitsov, for the informal discussions we have had and the help during thesis writting.

I would like to thank Junchen Pei, for the useful discussions and for the calculations with HFBAX code.

I would like to thank Yue Shi, for the his questions related to HFODD.

Special thanks to Prof. Dimiter Balanbanski, who gave me the opportunity to do doctoral research in University of Tennessee and Oak Ridge National Laboratory.

Abstract

The thesis studies the bulk deformation properties of the Skyrme nuclear energy density functionals. Following simple arguments based on the leptodermous expansion and liquid drop model, the current research applies the nuclear density functional theory to assess the role of the surface symmetry energy in nuclei. To this end, one can validate the commonly used functional parametrizations against the data on excitation energies of superdeformed band-heads in Hg and Pb isotopes, and fission isomers in actinide nuclei. After subtracting shell effects, the results of our self-consistent calculations are consistent with macroscopic arguments and indicate that experimental data on strongly deformed congurations in neutron-rich nuclei are essential for optimizing future nuclear energy density functionals. The resulting survey provides a useful benchmark for further theoretical improvements. Unlike in nuclei close to the stability valley, whose macroscopic deformability hangs on the balance of surface and Coulomb terms, the deformability of neutron-rich nuclei strongly depends on the surface-symmetry energy; hence, its proper determination is crucial for the stability of deformed phases of the neutron-rich matter and description of fission rates for r-process nucleosynthesis. The results and consequent discussions from the thesis were published in Ref. [134].

Contents

List of Figures

Chapter 1

Introduction

Atomic nuclei are self-bound systems of strongly interacting nucleons (protons and neutrons). In general, the strong interaction is described by quark-gluon degrees of freedom within Quantum Chromodynamics (QCD). QCD is a high-energy Gauge Field Theory based on an effective Lagrangian with $\mathrm{SU}_{\mathbf{color}}(3)$ symmetry group [1]. It is a very successful theory with a large variety of physics applications. However, QCD is still not able to describe the low energy-density domain where atomic nuclei are.

In the strongly non-perturbative case of low energy-density, the inter-nucleon interaction can be derived from the non-relativistic Effective Field Theory (EFT), where quark-gluon degrees of freedom can be represented by virtual effective meson exchanges. EFT uses an effective meson-exchange Lagrangian and series of time-ordered Feynman diagrams obtained by perturbation theory in momentum space, up to a given cut off Ref. [2]. Within EFT, matrix elements (both local and non-local) Ref. [3] of a given interaction can be written as series of two-body and many-body $\mathrm{N^2LO}$ terms. In this way, one can systematically build a set of effective potentials. Currently, such potentials are widely used in nuclear physics. There are several major methods which apply effective potentials to study quantum many-body problems, such as the ab-initio methods, the configuration interaction approaches (nuclear shell model), and the Density Functional Theory (DFT).

This thesis is focused on the macroscopic properties of heavy neutron-rich deformed nuclei. These exotic nuclei, lying far from, β-stability line, are important for nuclear physics and nuclear astrophysics Ref. [4]. The special attention is paid to the impact of the surface

symmetry energy on deformation properties of heavy neutron-rich nuclei. As we emphasize surface symmetry energy has a profound impact on deformation-dependent phenomena such as fission. Unfortunately, this important quantity has been poorly described by nuclear theory.

There are three main motivations of the current research:

- Development of new generation of DFT energy density functionals with better controlled deformation properties [135];
- Precise calculations of fission barriers and fission pathways based on DFT [135];
- Extrapolations to neutron rich heavy nuclei: competition between astrophyscial r-process and fission [23, 126, 127].

The nuclear DFT expresses the nucler binding energy by minimizing the energy density functional (EDF) that is defined through the energy density of the system. The binding energy of a finite nucleus of mass number ($A = N + Z$) and neutron excess $I = (N - Z)/A$ can be split into a smooth function of I and A (macroscopic liquid drop term), and a quantal shell correction term by means of the Strutinsky energy theorem Ref. [95,96]. This theorem provides a link between the self-consistent DFT and the macroscopic-microscopic models Ref. [41–44] Nuclear energy density functionals are usually developed by optimizing the low energy coupling constants to describe experimental data of nuclei and pseudo-data characterizing nuclear matter Ref. [45–49, 91, 92]. In this way, DFT energy contains both "bulk" (liquid drop) and "local" (shell effects) terms. As shown schematically in Fig.1.1, deformation energy of the nucleus as predicted by nuclear DFT is strongly affected by shell effects, which are responsible for the presence of superdeformed states and fission barriers.

The research described in this thesis is a continuation of Ref. [5, 54, 55] which employ a polynomial expansion of the liquid drop with respect to the inverse nuclear radius and neutron excess (leptodermous expansion). In the lowest order, leptodermous expansion contains mainly volume, symmetry, surface, surface-symmetry, curvature, direct Coulomb and exchange Coulomb terms. The volume and symmetry terms are related to the infinite nuclear matter properties, and they are fairly well determined. Surface energy can

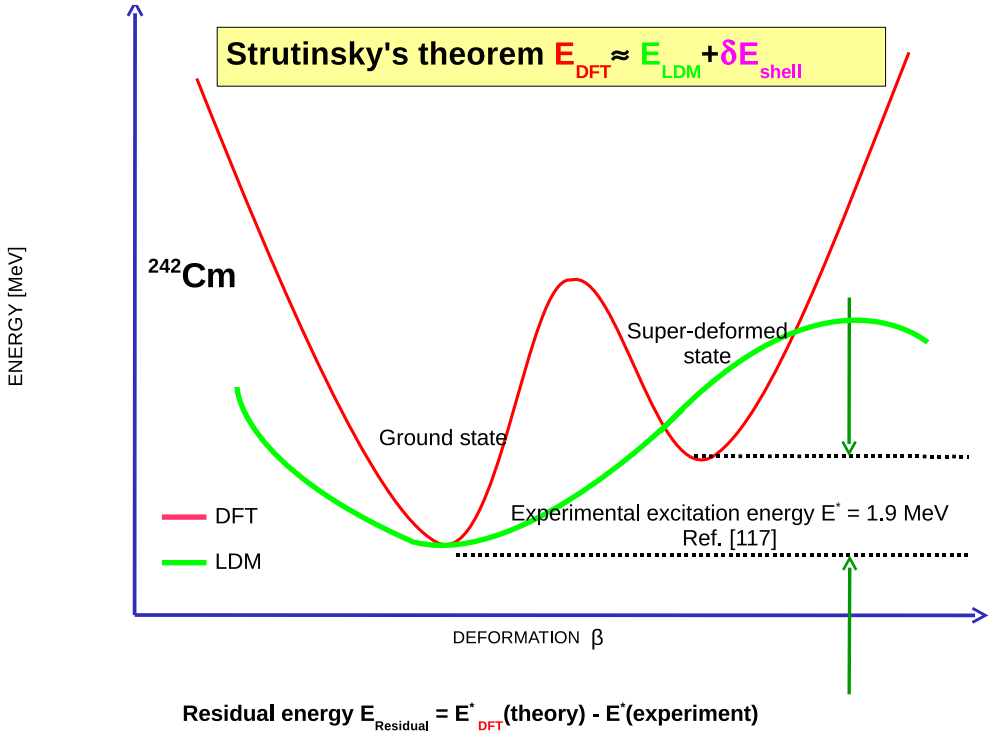

Figure 1.1: Binding energy versus quadrupole shape deformation predicted by the nuclear DFT (red). The green line represents the corresponding macroscopic LDM energy. The difference between DFT and LDM results can be atributed to shell effects. The shell energy dramatically effects the fission barrier and may produce superdeformed secondary metastable minima (fission isomers).

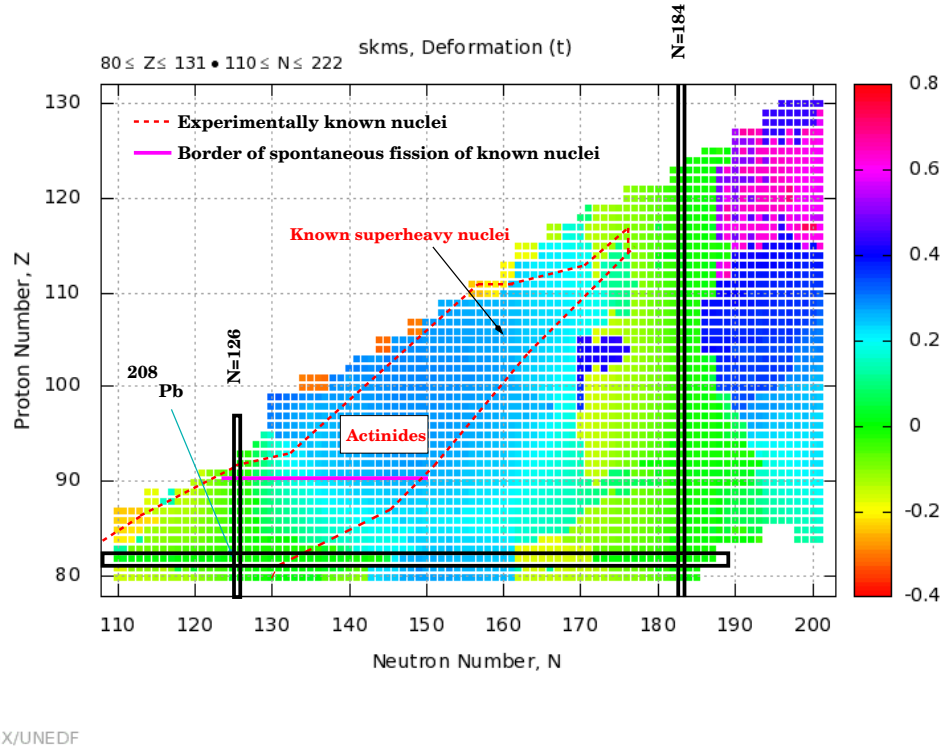

Figure 1.2: Ground state quadrupole deformation in the regions of the heaviest nuclei calculated in the DFT-SkM* model of Ref. [13]. The red dashed line indicates the approximated borders experimentally known nuclei and the purple solid line is the approximated threshold for spontaneous fission. Many neutron-rich deformed nuclei lie on the path of the astrophysical r-process; their fission rates are affected by the surface symmetry energy.

be determined from global nuclear properties such as masses, radii, and giant dipole resonances. The work Ref. [55] on leptodermous expansion of very large nuclei demonstrated that the surface-symmetry parameter a_{ssym} is poorely determined and its variations are large between different EDF parametrizations.

The thesis research investigated the leptodermous expansion in the case of heavy deformed nuclei. We found that variations of the surface-symmetry energy between different EDF parametrizations results in large fluctuations of the deformation energy of the order of a few MeV. Those are significant changes that can affect the theoretical predictions for deformed neutron-rich nuclei Ref. [14, 15, 17–23, 25–27, 126, 127].

The experimental data in the regions of neutron-rich heavy nuclei are either scarce or nonexistent. Many modern accelerator facilities explore the neutron-rich nuclei by experiments with exotic beams. These experiments inform theory by providing observables such as nuclear masses, radii, shell structure, collective effects, etc. However, there are regions of heavy nuclei ($A > 208$) well beyond the current experimental reach. Figure 1.2 nicely illustrates this point by displaying DFT predictions Ref. [13] for the ground state deformations of heavy nuclei with $Z > 80$ obtained with the SkM* EDF Ref. [106]. All experimentally known nuclei are shown in the region within the red dashed borders. Figure 1.2 also shows the neutron shell $N = 184$ which is predicted magic in some models. The purple line represents the approximate experimental border of spontaneous fission. Fission has a major impact on the astrophysical r-process and the abundance of the heaviest nuclei due to the recycling process. This research discusses theoretical extrapolations from the region of the experimentally known actinides towards the unknown neutron-rich isotopes, where the surface-symmetry energy becomes essential.

Within LDM, symmetry and surface-symmetry coefficients are correlated; hence they cannot be separated individually from the total energy of the nuclear liquid drop. Nevertheless, surface-symmetry energy can be constrained by strongly deformed configurations. This is what we do here: using self-consistent DFT we study the excitation energies of superdeformed (SD) states in the Hg-Pb region and actinides to separate and assess this elusive component of nuclear binding.

The results obtained in the thesis indicate that the surface-symmetry energy is as important as Coulomb energy for the deformation properties and the fissility of very neutron-rich nuclei. This suggests that experimental data on highly deformed neutron-rich nuclei are key for optimizing the modern EDFs.

The benchmark nuclei used in the calculations are: ^{192,194}Hg, $^{192-196}$Pb, ^{236,238}U, ^{240}Pu, and ^{242}Cm. For those systems, reliable experimental data on SD states exist Ref. [118–122, 124]. The methology applied in this work relied on the development of two essential technical elements:

- Development of a procedure that accurately extracts shell corrections from self-consistent energies by employing the Strutinsky's renormalization procedure;

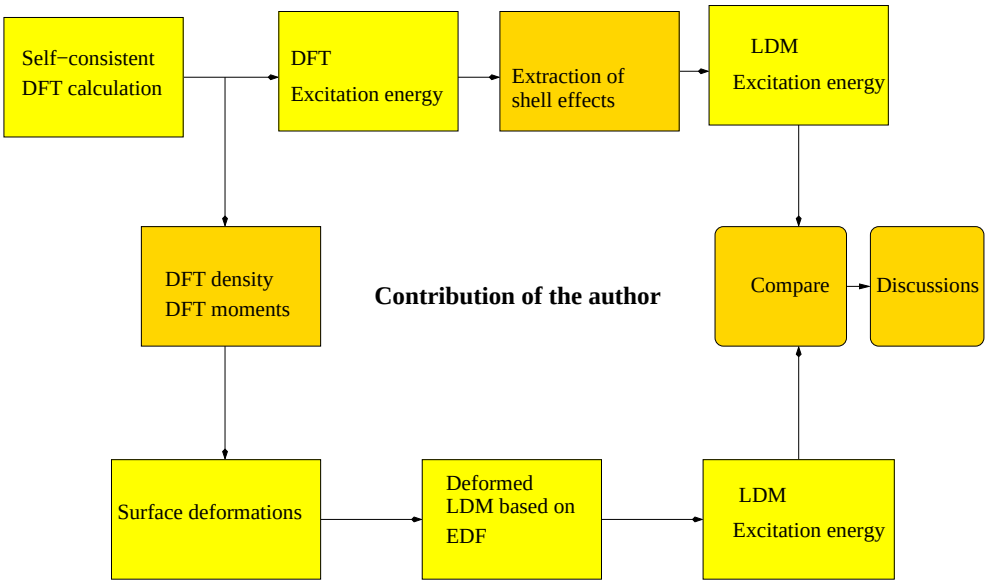

Figure 1.3: Schematic representation of the applied methology and the developed DFT-LDM interface.

- Development of a procedure that calculates nuclear shape deformations using the self-consistent densities.

Figure 1.3 illustrates the general methology used in this work and the DFT-LDM interface I developed and applied. The application of DFT-LDM interface was made as follows:

- HFB calculations of the excitation energy of superdeformed states and fission isomers in ^{192,194}Hg, ^{192,194,196}Pb, and ^{236,238}U, ^{240}Pu, ^{242}Cm. Comparing with the experimental data and average RMS deviation;
- Exctraction of the shell correction energy;
- Comparing the results with LDM using surface deformations as control parameters. Looking for surface-symmetry energy in the results;
- HFB and CHF calculations of the excitation energy of fission isomers in very neutron-rich Uranium isotopes;
- Extraction of the shell correction energy;

- Comparing with LDM. Large-scale trends of the surface-symmetry energy.

This thesis is organized as follows: Chapter 2 contains the essentials of DFT and LDM; Chapter 3 contains the numerical methods and procedures used; Chapter 4 presents the results for ^{192,194}Hg, ^{192,194,196}Pb, and ^{236,238}U, ^{240}Pu, ^{242}Cm; Chapter 5 discusses the predictions for very neutron-rich U isotopes that are expected to participate the fission recycling phase of the r-process. Finally, conclusions and perspectives are contained in Chapter 6.

Chapter 2

Theory

2.1 Energy Density Functional and HFB Equations

2.1.1 Density Functional Theory

In the original formulation of the Hohenberg-Kohn theorem Ref. [56] the average energy of a many-electron system can be written as

$$\bar{H} = \int d^3\mathbf{r}\mathcal{H}\left[\rho(\mathbf{r})\right] + \int d^3\mathbf{r} v_{ext}(\mathbf{r})\rho(\mathbf{r}), \tag{2.1}$$

where $\bar{H}$ is the mean energy of the system, $\mathcal{H}\left[\rho(\mathbf{r})\right]$ is the energy density, which depends on the density $\rho(\mathbf{r})$ of the system and $v_{ext}(\mathbf{r})$ is the external potential for the electrons. In the nuclear DFT, there is no external potential $v_{ext}(\mathbf{r})$ because the nucleus is a self-bound system of nucleons. Consequently, the EDF $\mathcal{H}\left[\rho(\mathbf{r})\right]$ can in principle be derived from an effective interaction. The effective nucleon-nucleon interaction has both local and non-local terms. Some nuclear EDF use only the local terms (local density approximation or LDA). Such is the case of the Skyrme EDFs Ref. [61].

The coupling constants of EDFs are usually obtained by optimizing calculated observables to experimental data. Since there are many fitting protocols, there are many Skyrme EDFs and they have different predictive power. Recently, the Universal Nuclear Energy Density Functional (UNEDF) collaboration has been set up to develop spectroscopic-quality EDFs rooted in the theory of the nuclear force Ref. [50].

2.1.2 Nuclear Effective Interactions

In the case of the Skyrme EDF Ref. [61], $\mathcal{H}\left[\rho(\mathbf{r})\right] = \mathcal{H}_{Kin} + \mathcal{H}_{Coulomb} + \mathcal{H}_{Skyrme}$. The term $\mathcal{H}_{Skyrme}$ originates from the Skyrme interaction, which is given by the expression (see Ref. [61])

$$\begin{aligned}\hat{V}\left(\mathbf{r'_1 s'_1 t'_1 r'_2 s'_2 t'_2}, \mathbf{r_1 s_1 t_1 r_2 s_2 t_2}\right) = &\left\{ t_0 \left(\hat{\delta}^\sigma + x_0 \hat{P}^\sigma\right) + \frac{t_3}{6}\left(\hat{\delta}^\sigma + x_3 \hat{P}^\sigma\right)\rho_0^\alpha \left[\frac{1}{2}\left(\mathbf{r_1} + \mathbf{r_2}\right)\right]\right\} \times \\ &\times \left(\hat{\delta}^\sigma \hat{\delta}^\tau - \hat{P}^\sigma \hat{P}^\tau \hat{P}^x\right)\hat{\delta}_{12} \\ + &\left\{ \frac{t_1}{2}\left(\hat{\delta}^\sigma + x_1 \hat{P}^\sigma\right)\left[\hat{\mathbf{k}}'^{\mathbf{2}} + \hat{\mathbf{k}}^{\mathbf{2}}\right] + \frac{1}{2} t_e \left[\hat{\mathbf{k}}'^* \cdot \hat{\mathsf{S}} \cdot \hat{\mathbf{k}}^* + \hat{\mathbf{k}} \cdot \hat{\mathsf{S}} \cdot \hat{\mathbf{k}}\right] + t_2 \left(\hat{\delta}^\sigma + x_2 \hat{P}^\sigma\right)\hat{\mathbf{k}}'^* \cdot \hat{\mathbf{k}}\right\} \times \\ &\times \left(\hat{\delta}^\sigma \hat{\delta}^\tau - \hat{P}^\sigma \hat{P}^\tau \hat{P}^M\right)\hat{\delta}_{12} \\ &+ \left\{ t_0 \hat{\mathbf{k}}'^* \cdot \hat{\mathsf{S}} \cdot \hat{\mathbf{k}} + i W_0 \mathbf{S} \cdot \left[\hat{\mathbf{k}}'^* \times \hat{\mathbf{k}}\right]\right\}\left(\hat{\delta}^\sigma \hat{\delta}^\tau - \hat{P}^\sigma \hat{P}^\tau \hat{P}^M\right)\hat{\delta}_{12}\end{aligned} \tag{2.2}$$

where $\hat{\delta}_{12} = \delta(\mathbf{r'}_1 - \mathbf{r}_1)\delta(\mathbf{r'}_2 - \mathbf{r}_2)\delta(\mathbf{r}_1 - \mathbf{r}_2)$. In expression (2.2) the variables r, s, t are respectively the coordinate, spin, and isospin of a nucleon; $\hat{\mathbf{k}}$ is the relative momentum; and $\hat{P}^{\tau,\sigma}$ is the (iso)spin-exchange operator. $\hat{P}^M = -\hat{P}^\sigma \hat{P}^\tau$ is the Majorana operator, which is related to the Pauli principle. Since nucleons are fermions, their wave-functions are anti-symmetric when permutations over the variables r, s, t are taken. In terms of exchange operators, anti-symmetrization is given by $\hat{P}^r \hat{P}^\sigma \hat{P}^\tau = -1$, where $\hat{P}^r$ is the operator that exchanges the spacial coordinate r. The relation between the Majorana operator and coordinate-exchange can be written as $\hat{P}^M = \hat{P}^\sigma \hat{P}^r \hat{P}^\sigma$. $\mathbf{S}$ and S represent spin operators (vector/tensor) and $t_{i=0,1,2,3}$, $x_{i=0,1,2,3}$, and W_0 (spin-orbit coupling constant) are free parameters adjustable to experiment. What can be seen from (2.2) is that the Skyrme interaction has isospin dependence (for example via the isospin exchange operator) which produces the isovector densities of the functional. These isovector densities control the evolution of the properties of nuclei as a function of neutron excess.

2.1.3 Nuclear Energy Density Functional

From expression (2.2), one can show that by taking the expectation value of the the Skyrme interaction (2.3), one can write the energy-density (EDF) $\mathcal{H}(\mathbf{r})$ as

$$\mathcal{H}(\mathbf{r}) = \frac{\hbar}{2m}\tau_0(\mathbf{r}) + \mathcal{H}(\mathbf{r})_{Coul} + \sum_{0,1}\chi_t(\mathbf{r}). \tag{2.3}$$

with $\chi_t(\mathbf{r})$ being the particle-hole energy density. The latter one contains isoscalar and isovector components, denoted by the index $t = 0, 1$ [1], due to the presence isoscalar and isovector densities $\rho_0 = \rho_n + \rho_p$ and $\rho_1 = \rho_n - \rho_p$.

Both terms $\chi_{0,1}$ depend on the normal density ρ, the spin density s, and the kinetic density τ, as well as coupling constants C_i. They are directly related to the parameters $t_{i=0,1,2,3}$, $x_{i=0,1,2,3}$, and W_0 of the original Skyrme interaction (2.2) Ref. [61]. Other involved densities are the spin-current,tcurrent, spin-kinetic, and tensor-kinetic densities. Their expressions can be found in Ref. [61]. Expression (2.3) contains both the time-even (time-reversal symmetry) and time-odd parts of the Skyrme EDF. The time-odd part is active when time-reversal symmetry is broken. This part of the functional must then be taken into account when applying DFT to states with non-zero spin. For simplicity, the current research is restricted to even-even nuclei with zero angular momentum, where time-odd fields are not present. More information about the time-odd parts of the EDF can be found in Ref. [45, 61].

The parameters of the Skyrme interaction (2.2) $x_i, t_{i=0,1,2,3}$ are adjusted directly to the nuclear matter properties and experimental data, by various optimization methods. The experimental data used in such fits usually include nuclear masses, single-particle levels, giant resonances, and charge radii. Only three functionals: SkM* Ref. [106], BSk6 Ref. [109], and HFB-14 Ref. [128] were fitted indirectly to very deformed nuclei, by considering experimental fission barrier of ^{240}Pu.

[1] The difference between isoscalar and isovector densities is related with the isospin dependence $\sim \sum \hat{\rho}\hat{\tau}$, where τ denotes the vector of isospin Pauli matrices. See Ref. [61] for further details.

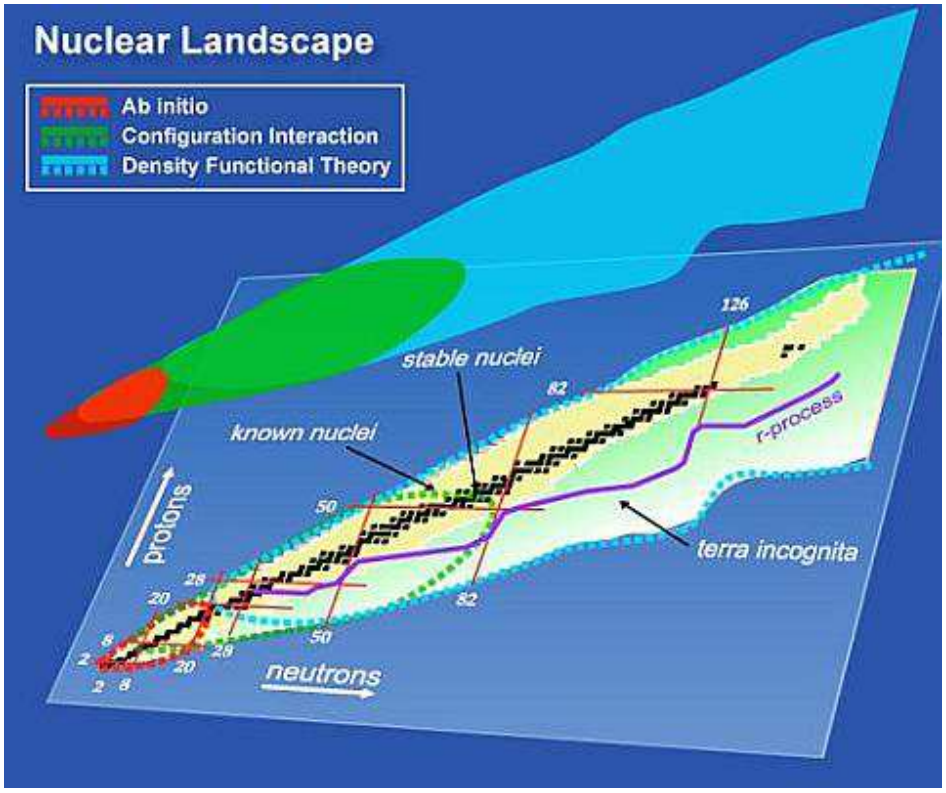

Figure 2.1: Nuclear landscape and the corresponding theories [117]. For the past 30 years, different Skyrme functionals have been used in large-scale DFT nuclear structure calculations with considerable success primarly for medium and heavy nuclei. For light and medium nuclei, ab initio methods and configurational interactions have been very successful. However, despite the intense work on connections between ab initio methods and DFT (for example the Density Matrix Expansion method Ref. [53]), no comprehensive theoretical picture has emerged yet.

2.1.4 The Hartree-Fock Method

The density-dependent Hartree-Fock (HF) method is an independent-particle approximation where the expectation value of the effective many-body Hamiltonian is computed within a Slater determinant of single-particle wave functions. The total energy is calculated by minimizing the total energy-density with respect to the density of the system by considering small variations $\rho + \delta\rho$. This can be achieved by solving self-consistent HF equations. The single-particle occupation numbers are either 1 (hole states) or 0 (particle states).

2.1.5 Pairing Correlations

When the particle-particle correlations are involved, the Fermi surface is diffused and single-particle occupation numbers are between 0 and 1. Pairing correlations between pairs of particles can be described in the Bardeen-Cooper-Schrieffer (BCS) theory. In a simple HF+BCS scheme, correlated BCS states are built on top of the HF states, and the minimization is carried out separately for HF and BCS. The full generalization of the variational principle that includes pairing correlations is achieved using the Hartree-Fock-Bogoliubov method [72].

2.1.6 The Hartree-Fock-Bogoliubov (HFB) Approach

The HFB method employs quasi-particle wave-functions using a set of unitary transformations known as Bogoliubov transformations. In the HFB theory, the average energy E_{HFB} is defined by the expectation value of the nuclear Hamiltonian with respect to the quasiparticle vacuum $|\Psi\rangle$:

$$E_{HFB} = \bar{H} = \langle\Psi|H|\Psi\rangle. \tag{2.4}$$

the quasiparticle states are eigenvectors of HFB equations:

$$\begin{pmatrix} \hat{h} - \lambda & \hat{\breve{h}} \\ -\hat{\breve{h}}^* & -\hat{h}^* + \lambda \end{pmatrix} \begin{pmatrix} U \\ V \end{pmatrix} = E \begin{pmatrix} U \\ V \end{pmatrix}.$$

The HFB energy is minimized with respect to the HF density $\hat{\rho}$ and pairing density $\breve{\hat{\rho}}$. $\hat{h}(r's't', rst) = \delta\bar{H}/\delta\hat{\rho}$, and $\hat{\breve{h}}(r's't', rst) = \delta\bar{H}/\delta\breve{\hat{\rho}}^+$ (antisymmetric pairing potential); $\lambda = \lambda_i\hat{\tau}^3$ is the Fermi energy at given isospin τ ($i = p$ for protons, $i = n$ for neutrons); E

is the diagonal matrix of quasiparticle energies. U and V are matrices which define the quasi-particle wave function. As usual, $\mathbf{r}$ denotes the position; s spin; and t isospin.

2.1.7 Mixed Pairing Interaction

As mentioned earlier, the local energy density $\mathcal{H}(\mathbf{r})$ contains both particle-hole and particle-particle contributions. The particle-particle term of the energy density represents the pairing channel. For the Skyrme effective functional, the particle-particle term has, in principle, a similar formal structure to the particle-hole part, but the density $\hat{\rho}$ is replaced by $\hat{\tilde{\rho}}$. In practice, the pairing term is simplified by using a delta-function interaction, i.e.

$$\hat{\tilde{h}}(\mathbf{r}^{'}, \mathbf{r}) = f(\mathbf{r})\delta(\mathbf{r} - \mathbf{r}^{'}), \tag{2.5}$$

where

$$f(\mathbf{r}) = \frac{1}{2}V_0 \left[1 - V_1 \left(\frac{\rho(\mathbf{r})}{\rho_0}\right)^{\alpha}\right]. \tag{2.6}$$

Usually $\alpha = 1$, and V_1 is 0, 1, or 1/2 for volume, surface or mixed-type pairing. In this work, mixed pairing correlations have been used with a dependence on the isoscalar density Ref. [51, 52].

The value of the parameter V_0 is obtained by fitting the average pairing gap in a nucleus, where the experimental odd-even energy is known. By employing such a fit for each EDF parametrization, a specific value of the pairing strength V_0 can be obtained. Figure 2.2 shows the dependence of the neutron pairing gap in ^{120}Sn on the pairing strength V_0 in the case of 20 different Skyrme EDFs, used in this study. The experimental neutron pairing gap is $\Delta_n = 1.245[MeV]$. In this way V_0 can be found for each EDF. The nucleonic pairing has a major impact on predicted excitation energies of SD states (see Section 4.2).

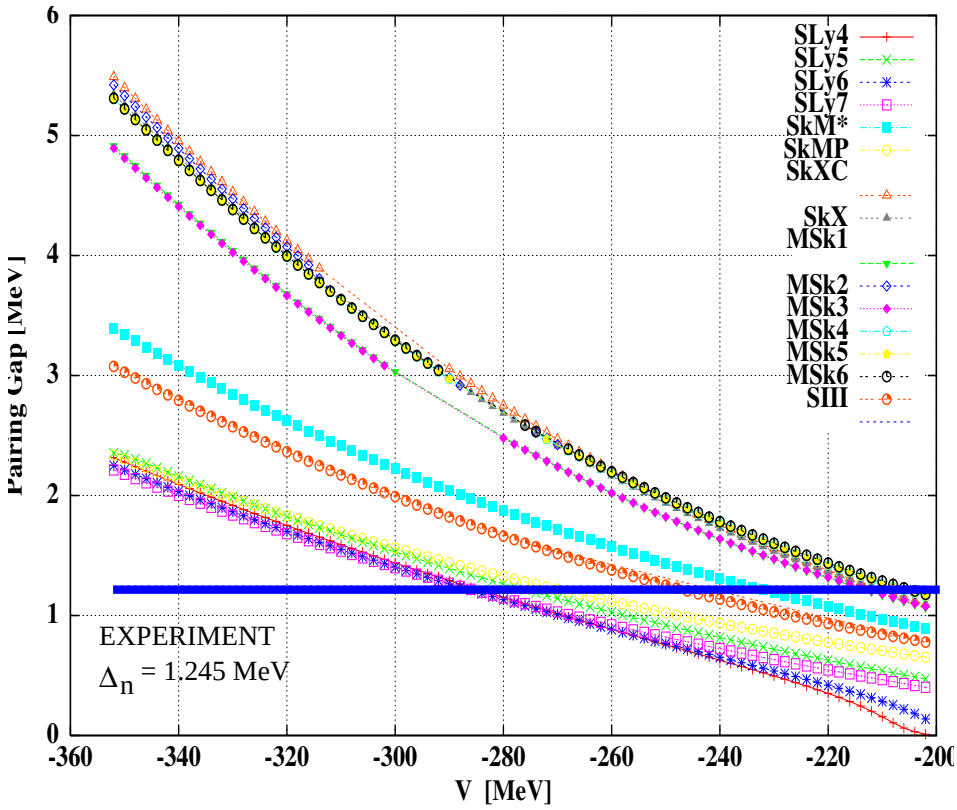

Figure 2.2: Calculated pairing gaps in ^{120}Sn as a function of the pairing strength V_0 for various Skyrme functionals. The experimental pairing gap in ^{120}Sn is 1.245 MeV. Missing points: not converged HFB results.

2.2 Liquid Drop Model

The goal of this research is to study how standard Skyrme functionals describe surface effects in nuclei, in particular the isospin-dependent surface-symmetry component of the total bulk energy. Since surface-symmetry energy plays an important role in stability of the heavy neutron rich nuclei, the hope is that this will provide better theoretical understanding of exotic nuclei participating in the stellar nucleosynthesis.

2.2.1 Leptodermous Expansion of the Nuclear Binding energy

It is useful to begin the discussion from the equation of state (EoS) of the asymmetric infinite nuclear matter, which gives the energy-density per particle. Its conventional form is a Taylor expansion Ref. [5, 37–40]

$$\frac{E}{A} \approx -a_{\rm vol} + \frac{K_\infty}{18\rho_0^2}\left(\rho-\rho_0\right)^2 + ... + \left[a_{\rm sym} + \frac{p}{\rho_0}\left(\rho-\rho_0\right) + ...\right] I^2 + .., \tag{2.7}$$

where $\rho_0 \approx 0.16{\rm fm}^{-3}$ is the saturation density, $a_{\rm vol}$ is the volume energy coefficient, $a_{\rm sym}$ is the symmetry energy coefficient and K_∞ is the incompressibility parameter:

$$K_\infty = 9\rho_0^2 \frac{d^2}{d\rho_0^2}\frac{E}{A}.$$

All these parameters have direct connection to the parametrization of the effective interaction or, alternatively, to the EDF. The next step is to assume that a nucleus is a finite chunk of nuclear matter. Introducing nuclear radius $\sim A^{1/3}$ and nuclear surface $\sim A^{2/3}$, one can obtain

$$E_{\rm LDM}\left(A,I\right) = A\left(-a_{\rm vol} + \frac{a_{\rm surf}}{A^{1/3}} + \left[a_{sym}^{Vol} - \frac{a_{sym}^{Surf}}{A^{1/3}} + ...\right]\left(I^2+...\right) + ...{\rm next-leading-order}\right). \tag{2.8}$$

Expression (2.10) is known as the Liquid Drop Model mass formula [5], which gives the macroscopic binding energy of a finite quantum drop of protons and neutrons. The polynomial expansion of (2.8) can be written in a more generalized way by invoking powers of the inverse radius $A^{-1/3}$ and neutron excess I as listed in Table 2.1. Each term has a macroscopic physical interpretation as volume, surface, symmetry, curvature, surface-symmetry, etc. Due to the presence of protons, Eq. (2.8) has to include the Coulomb energy as well.

Reordering the various terms of the expansion (2.8), the general form of the LDM

1	$A^{-1/3}$	$A^{-2/3}$
I^2	$I^2A^{-1/3}$	$I^2A^{-2/3}$
I^4	$I^4A^{-1/3}$	$I^4A^{-2/3}$

Table 2.1: LDM expansion terms, see Ref. [54] for details.

binding energy per nucleon reads Ref. [55]:

$$E_{\mathrm{LDM}}(A,I) = A\left(a_{\mathrm{vol}} + a_{\mathrm{sym}}I^2 + a_{\mathrm{surf}}A^{-1/3} + a_{\mathrm{curv}}A^{-2/3} + a_{\mathrm{ssym}}I^2A^{-1/3} + a^{(2)}_{\mathrm{sym}}I^4\right), \tag{2.9}$$

This systematic expansion of the liquid drop energy in powers of the mass and neutron excess is known as the "leptodermous expansion".

2.2.2 The Symmetry Energy

Expression (2.9) is valid for spherical nuclei and is a sum of terms that can be associated either with infinite nuclear matter or finite-size surface effects. The infinite nuclear matter terms are the volume a_{vol} and the symmetry energy $a_{sym}I^2$. The finite-size terms are the surface $a_{surf}A^{-1/3}$, the curvature $a_{curv}A^{-2/3}$, and the surface-symmetry $a_{ssym}I^2A^{-1/3}$ energy.

The total symmetry energy is the sum of the volume symmetry $a_{sym}I^2$ and surface-symmetry $a_{ssym}I^2A^{-1/3}$ terms

$$\frac{E_{sym}}{A} = \left(a_{sym} + \frac{a_{ssym}}{A^{1/3}}\right) I^2. \tag{2.10}$$

The symmetry energy of a finite nucleus is a macroscopic feature with volume and surface terms, but it can also be related to the nucleon-nucleon interaction, or the EDF. In the case of the Skyrme EDF, the *volume* symmetry term a_{sym} is

$$a_{\mathrm{sym}} = \frac{1}{2}\frac{\partial^2\mathcal{H}/\rho_0}{\partial I^2}\bigg|_{I=0} = \frac{1}{3}\left[\frac{\hbar^2}{2m} + \left(C_0^\tau + 3C_1^\tau\right)\rho_0\right]\beta\rho_0^{2/3} + C_1^\rho[\rho_0]\rho_0, \tag{2.11}$$

where $\beta = \left(3\pi^2/2\right)^{2/3}$, and ρ_0 is the saturation density. One clearly sees that the symmetry energy depends on both the isoscalar and isovector components of the functional. The isoscalar component is related to $\frac{\hbar^2}{2m}$ and the C_0^τ parameter; the isovector part is related to C_1^τ. Here, the link between the parametrization of the Skyrme functional and the symmetry energy is analytical. Also, it is clear that surface symmetry energy is naturally derived

from the total symmetry energy since it is caused by finite-size effects (see Figure 2.3). However, there is no analytical expression for the *surface* symmetry energy, as a function of the parameters of the functional. In fact, all parameters $a_{vol}, a_{surf}, a_{sym}, a_{curv}, a_{ssym}$ depend on the parametrization of the microscopic effective interaction, and for all those parameters corresponding to surface effects, this dependence is non-analytical and can only be extracted by a numerical fit. In the work of Ref. [55] these parameters were extracted from Skyrme Hartree-Fock calculations for nuclei with an extremely large number of nucleons (A>2000), where Coulomb energy had been removed. Table 2.2 presents the values of the coefficients in (2.9) corresponding both to infinite nuclear matter and finite size effects for nine Skyrme functionals.

Force	$a_{\rm sym}$	$a_{\rm ssym}$	a_{sur}	Force	$a_{\rm sym}$	$a_{\rm ssym}$	a_{sur}
SkM*	30.04	-52	17.6	NL1	43.48	-110	18.8
SkP	30.01	-45	18.2	NL3	37.40	-86	18.6
BSk1	27.81	-36	17.5	NL-Z	41.74	-125	17.8
BSk6	28.00	-33	17.3	NL-Z2	39.03	-90	17.4
SLy4	32.01	-54	18.4				
SLy6	31.96	-51	17.7	LDM$^{(1)}$	30.56	-48.6	21.1
SkI3	34.84	-75	18.0	LDM$^{(2)}$	29.28	-38.4	19.4
SkI4	29.51	-34	17.7	LSD	28.82	-38.9	17.0
SkO	31.98	-58	17.3				

Table 2.2: Surface and surface-symmetry coefficients (in MeV) entering the LDM expression for the binding energy as extracted in Ref. [55]. References for the Skyrme forces: SkM* Ref. [106], SkP Ref. [107], BSk1 Ref. [108], BSk6 Ref. [109], SLy4-SLy6 Ref. [110], SkI3-SkI4 Ref. [111], SkO Ref. [112]. For the relativistic Lagrangians: NL1 Ref. [113], NL-Z Ref. [114] and NL-Z2 Ref. [115]. For the LD: LDM$^{(1)}$ Ref. [4], LDM$^{(2)}$-LSD Ref. [116].

Table 2.2 suggests that the parameters of the infinite nuclear matter terms fluctuate very slowly between the Skyrme interactions. These small fluctuations have large effect on the energy (2.8) because in many-body systems they are "amplified" by the particle number A Ref. [55].

The surface coefficients manifest even larger differences than those associated with the volume terms. This is especially true for the value of the surface-symmetry coefficient a_{ssym}. Surface-symmetry is related to the finite-size liquid drop but it has a complicated connection to all C coupling constants of the energy-density $\mathcal{H}(r)$. The numerical extraction of the a_{ssym} is based on extrapolation of the symmetry coefficient a_{sym} from nuclear matter to finite A values based on average integration with respect to the neutron excess I as shown in Ref. [55]. The slope of the extrapolation with respect to $A^{-1/3}$ gives the value of the a_{ssym}. The extrapolation excluded the Coulomb energy.

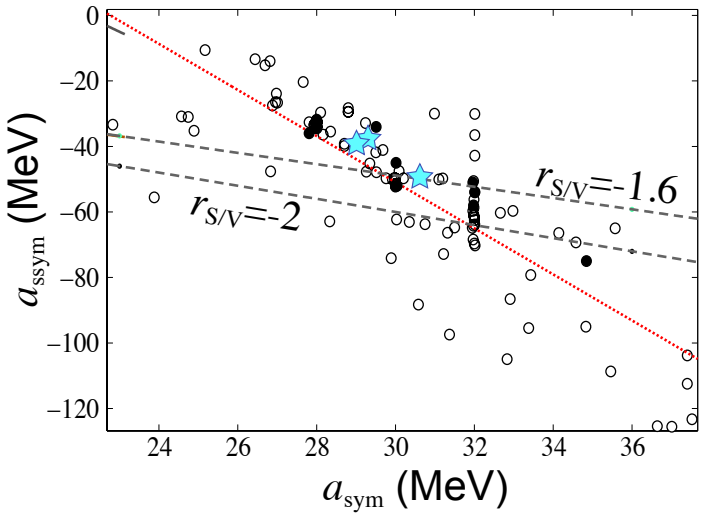

Figure 2.3: Relation between the symmetry a_{sym} and surface-symmetry a_{ssym} coefficients for the Skyrme interactions presented in Table 2.2 (dots) and Ref. [5] (circles). The phenomenological LDM from Table 2.2 are presented with stars. The ratio is $r_{S/V} = -2$ from the hydrodynamical estimated Ref. [59] and -1.6 (dashed lines) from the mass estimate Ref. [12, 60]. The total linear fit from Ref. [5] is the dotted line.

The correlation (2.10) between the surface-symmetry coefficient a_{ssym} and the volume symmetry coefficient a_{sym} is shown in Figure 2.3 for various parametrizations of the Skyrme interaction (Table 2.2). Such a correlation was established in early Hartree-Fock (HF) and extended-Thomas-Fermi calculations Ref. [75–78]. It was later shown that the correlation has an A-dependence Ref. [60]. The linear fit from Figure 2.3 can provide information about the ratio $r_{S/V} = \frac{a_{ssym}}{asym}$ which can be estimated from experiments that yield values

such as electric dipole strength distribution Ref. [31], masses Ref. [4, 29, 32, 33], masses and radii Ref. [30, 34, 35], and excitation energies of isobaric analog states and neutron separation energies Ref. [36]. For example, the $r_{S/V} \approx -1.7$ from experimental masses Ref. [58] and the electric dipole polarization data give $r_{S/V} \approx -1.65$ Ref. [12]. From Ref. [60] A-dependence yields $r_{S/V} = -1$ for $A \geq 12$, and -1.7 for $A \geq 50$. The main goal is the extraction of a_{ssym} from the experimental data of the ground-state. However, the results show that a_{ssym} cannot be constrained by these methods due to "contamination" from the other terms in (2.12).

2.2.3 Deformed Liquid Drops

An alternative method to extract the value of a_{ssym} by using LDM energy (2.9) is to use the excitation energy of highly-deformed nuclei. This is because the volume symmetry coefficient a_{sym} does not depend on the deformation, and the correlation between volume and surface symmetry coefficients can therefore be cancelled. In a deformed system, the binding energy per nucleon becomes:

$$\frac{E_{\rm LDM}}{A}(A,I;{\rm def}) = a_{\rm vol} + b_s a_{\rm surf} A^{-1/3} + a_{\rm sym} I^2 + b_{\rm curv} a_{\rm curv} A^{-2/3} + b_s a_{\rm ssym} I^2 A^{-1/3} + b_{\rm coul} \frac{3e^2 Z^2}{5 r_0 A^{4/3}} + \frac{5}{4}\left(\frac{3}{2\pi}\right)^{2/3} \frac{3e^2 Z^{4/3}}{5 r_0 A^{4/3}}, \tag{2.12}$$

where the deformation is introduced by the geometrical form factors $b_{surf,coul,curv}$ taken from Ref. [74]. Eq (2.12) can be used to compute deformation energy of deformed states. An important feature of (2.12) is that the high-order symmetry energy $a^{(2)}_{sym} I^4$ is omitted and the Coulomb and the Coulomb exchange energy $\frac{5}{4}\left(\frac{3}{2\pi}\right)^{2/3} \frac{3e^2 Z^{4/3}}{5 r_0 A^{2/3}}$ are shown. Neglecting the high-order symmetry energy is justified in realistic nuclei with $I << 1$, like those studied in this work. Contrariwise, a realistic description of nuclei requires properly taking Coulomb effects into account. The deformation excitation energy can be calculated by subtracting (2.12) for two different fixed deformations, i.e.

$$\frac{E^{\rm exc}_{\rm LDM}}{A}(A,I;{\rm def}) = \left(b_s - b_s'\right)\left(a_{\rm surf} + a_{\rm ssym} I^2\right) A^{-1/3} + a_{\rm curv}\left(b_{curv} - b_{curv}'\right) A^{-2/3} + \left(b_{coul} - b_{coul}'\right) \frac{3e^2 Z^2}{5 r_0 A^{4/3}}, \tag{2.13}$$

where one can see that volume terms from (2.12) do not appear. The contributors in (2.13) are all finite size terms.

In the LDM, the Coulomb potential is that of a uniformly charged sphere (or ellipsoid if there is deformation) which depends on the Wigner-Seitz radius r_0 calculated at the nuclear saturation density ρ_0, i.e. $r_0 = \sqrt[3]{\frac{3}{4\pi\rho_0}}$. Saturation density ρ_0 and r_0 depend on the Skyrme interaction. However, as will be discussed in Chapter 3, the LDM parameterizations obtained in Ref. [55] did not include the Coulomb potential: therefore, they cannot be compared directly to HFB calculations, as the proper value for r_0 is unknown. Coulomb effects in HFB calculations cannot be removed easily either, as they are related to the local shell energy (single-particle levels) and introduce a "shift" in the excitation energy of the highly-deformed nuclei of the order of MeV. Therefore, one can use r_0 as a local control parameter, which introduces shell fluctuations into the LDM that in the spherical case Ref. [132] are small. The determination of r_0 is discussed in Chapter 3.

As it has been shown, the volume symmetry energy is cancelled in (2.13) because of its infinite matter character, but the contribution of surface-symmetry energy remains. So (2.13) can be used to calculate the excitation energy of deformed nuclei, and to extract a_{ssym}. In the present case, the deformation form factors $b_{surf,coul,curv}$ are not arbitrary; they are deduced from HFB calculations for the ground state, super-deformed and fission isomeric minima in realistic nuclei. The method used for this extraction is described in Chapter 3. The results are shown in Chapters 4 and 5.

Chapter 3

Methods, Developments, and their Justification

This chapter presents the methods and code developments that have been used to calculate the excitation energies of super-deformed states and fission isomers. These calculations involve basic technicalities related to the numerical convergence of HFB, the calculation of the macroscopic energy from HFB results, and the extraction of LDM deformations from the HFB densities.

This chapter is organized into three sections. The first section will present the Harmonic Oscillator basis expansion, which is used to expand the HFB wavefunctions in the used solvers. Because all observables depend on the size of the basis, one has to ensure that the basis is large enough so that the final observables are independent of employed basis. The second section shows the method of extraction of the macroscopic excitation energy by Strutinsky's Theorem. The last section presents the calculation of the Liquid Drop Model deformation parameters from the expectation value of the surface multipole moments operators.

3.1 Harmonic Oscillator Basis and Convergence Tests

The two codes used in the HFB and HF calculations were HFODD developed by Ref. [66, 67, 69, 70] and the HFBTHO code developed by Ref. [68]. HFODD uses an expansion

of the single-particle wave functions $\psi(\mathbf{r}\sigma)$ in the deformed HO wave functions $\phi_{n_x n_y n_z}(\mathbf{r}\sigma)$ in Cartesian coordinates:

$$\psi_i(\mathbf{r}\sigma) = \sum_{n_x=0}^{N_x} \sum_{n_y=0}^{N_y} \sum_{n_z=0}^{N_z} A_i^{n_x,n_y,n_z} \phi_{n_x n_y n_z}(\mathbf{r}\sigma), \tag{3.1}$$

where $N_{z,y,x}$ is the maximum number of HO shells in each of the three different Cartesian directions and σ is the projection on the spin of the z-axis for the nucleons. This section will show how this expansion is used in operator representation and how the final excitation energies and equilibrium deformations of nuclei depend on $N_{z,y,x}$ in (3.1). It will also present examples of other methods of solving HF(HFB), such as box-boundary HFB. The oscillator wave functions $\phi_{n_x n_y n_z}(\mathbf{r}\sigma)$ are a product of the separate wave functions of x, y, z, i.e.,

$$\phi_{n_x n_y n_z}(\mathbf{r}\sigma) = \phi_{n_x}(x)\phi_{n_y}(y)\phi_{n_z}(z) \otimes |\sigma\rangle, \tag{3.2}$$

with

$$\phi_{n_\mu}(x_\mu) = \sqrt{b_\mu} H^{(0)}_{n_\mu}(\xi_\mu) e^{-\frac{\xi_\mu^2}{2}}, \mu = 1, 2, 3. \tag{3.3}$$

The dimensionless variables $\xi_\mu = b_\mu x_\mu$, and b_μ are the oscillator constants $b_\mu = \sqrt{m\omega_\mu/\hbar}$. $H^{(0)}_{n_\mu}$ are polynomials coming from the orthogonal Hermite polynomials $H_n(\xi)$,

$$H^0_n(\xi) = \left(2^n n! \sqrt{\pi}\right)^{-1/2} H_n(\xi). \tag{3.4}$$

The normalization of $H^{(0)}_{n_\mu}$ is

$$\int_{-\infty}^{\infty} d\xi H^{(0)}_n(\xi) H^{(0)}_{n'}(\xi) e^{-\xi^2} = \delta_{nn'}. \tag{3.5}$$

By using expressions (3.1) through (3.5) one can write the matrix elements of any operator in the HO basis. The expressions are different for operators with derivatives and those without derivatives. In the simple case of operators without derivatives, the expressions of its matrix elements use the normalization form (3.5). Thus for an operator $\hat{O}(x, y, z)$ one has:

$$\langle n_x n_y n_z | \hat{O} | n_x^{'} n_y^{'} n_z^{'} \rangle = \sum_{k_x} C^{k_x}_{n_x n_x^{'}}(00) \sum_{k_y} C^{k_y}_{n_y n_y^{'}}(00) \sum_{k_z} C^{k_z}_{n_z n_z^{'}}(00) O_{k_x k_y k_z}, \tag{3.6}$$

where $C^{k_i}_{n_i n_i^{'}}(00)$ are the zero-order coefficients from the expansion

$$H^{(d)}_{n_\mu}(\xi) H^{(d^{'})}_{n_\mu^{'}}(\xi) = \sum_{k=0}^{n-n^{'}+d-d^{'}} C^k_{nn'}(dd^{'}) H^{(0)}_k(\xi), \tag{3.7}$$

and $O_{k_x k_y k_z}$ is given by the 3-fold integral

$$O_{k_x k_y k_z} = \int\int\int d\xi_x d\xi_y d\xi_z O\left(\frac{\xi_x}{b_x}, \frac{\xi_y}{b_y}, \frac{\xi_z}{b_z}\right) H^{(0)}_{k_x}(\xi_x) H^{(0)}_{k_y}(\xi_y) H^{(0)}_{k_z}(\xi_z) e^{-\xi_x^2 - \xi_y^2 - \xi_z^2}. \tag{3.8}$$

The integrals (3.8) are calculated by Gauss-Hermite quadratures. In HFODD all operators $O(x,y,z)$ needed to solve the Skyrme HFB problem can actually be represented as $O(x,y,z) = W(x,y,z)e^{-\xi_x^2-\xi_y^2-\xi_z^2}$, since they are linearly dependent on the density matrix ρ. In that case, one can have

$$O_{k_xk_yk_z} = \int\int\int d\xi_x d\xi_y d\xi_z W\left(\frac{\xi_x}{b_x},\frac{\xi_y}{b_y},\frac{\xi_z}{b_z}\right) H^{(0)}_{k_x}(\xi_x)H^{(0)}_{k_y}(\xi_y)H^{(0)}_{k_z}(\xi_z)e^{-2\xi_x^2-2\xi_y^2-2\xi_z^2}$$

$$= \frac{1}{\sqrt{8}}\int\int\int d\eta_x d\eta_y d\eta_z W\left(\frac{\eta_x}{b_x\sqrt{2}},\frac{\eta_y}{b_y\sqrt{2}},\frac{\eta_z}{b_z\sqrt{2}}\right) H^{(0)}_{k_x}(\frac{\eta_x}{\sqrt{2}})H^{(0)}_{k_y}(\frac{\eta_y}{\sqrt{2}})H^{(0)}_{k_z}(\frac{\eta_z}{\sqrt{2}})e^{-\eta_x^2-\eta_y^2-\eta_z^2}$$

$$= \sum_{l_x=1}^{L_x} G^{l_x}_{k_x}\sum_{l_y=1}^{L_y} G^{l_y}_{k_y}\sum_{l_z=1}^{L_z} G^{l_z}_{k_z} W\left(\frac{\eta_{l_x}}{b_x\sqrt{2}},\frac{\eta_{l_y}}{b_y\sqrt{2}},\frac{\eta_{l_z}}{b_z\sqrt{2}}\right) \quad (3.9)$$

where the matrices G^l_k involve the integration weights w_l as

$$G^l_k = \frac{w_l}{\sqrt{2}}H^{(0)}_k(\frac{\eta_l}{\sqrt{2}}), \quad (3.10)$$

$L_{x,y,z}$ are the numbers of Gauss-Hermite points, which are related to the maximum number of quanta in the HO basis, $L_i = 2N_i + 2$. All of these expressions show the mathematical representation of the operators within the HO basis and also show that the numerical results are related to the parameters of the basis, such as the number of oscillator shells N and the oscillator length b_μ. Therefore a test for convergence is needed which will prove that the final results do not change significantly with the basis. In the current work such a test was done for ^{240}Pu, where the ground state and fission isomer energies were calculated as a function of the number of oscillator shells N. An additional optimization over the oscillator length was performed (see Figure 3.1). The binding energies of the ground state and the fission isomer converge exponentially with respect to the number of oscillator shells N. For infinite HO large basis binding energy is constant. In the case of ^{240}Pu, HFBAX represents calculations in infinite basis size Ref. [85].

In the same way Figure 3.2 presents the trend of the fission isomer excitation energy $E_{isomer} - E_{GS}$ with the number of oscillator shells N. As shown in the figure, the convergence of both states is roughly exponential and results can be considered reasonably converged beyond 25 shells. The convergence of the excitation energies with respect to the number of oscillator shells N creates a numerical error. In the particular case of ^{240}Pu, the numerical error of the fission isomer excitation energy is $\Delta E_{excit} \approx 0.5MeV$ at 16 shells. In Figure 3.2, the exponential convergence is also compared to a calculation using the coordi-

nate space code HFBAX (infinite basis size) Ref. [85]. It is important to mention that the numerical error of the excitation energy is not a statistical error, but an error related to a well-defined exponential trend (as observed in Ref. [87] and [88]), which always decreases the energy. Therefore, the final error at 16 shells is not ± 0.5 MeV, but just -0.5 MeV.

In the HFB calculations, the fission isomer excitation energy was extracted with basis size $N_{\max} = 20$ oscillator shells, which is sufficient for strongly elongated systems (Figure 3.2). The cancellation of the errors mentioned above implies that the calculations do not need 25 shells. HFB calculations were done mainly with HFODD Ref. [66], because it is one of the best codes for fission calculations due to the symmetry breaking options. However, HFODD is slower than HFBTHO. HFBTHO uses a transformed harmonic oscillator basis (THO), which is derived from the HO, by unitary transformations and local-scaling point transformations (LST) Ref. [71].

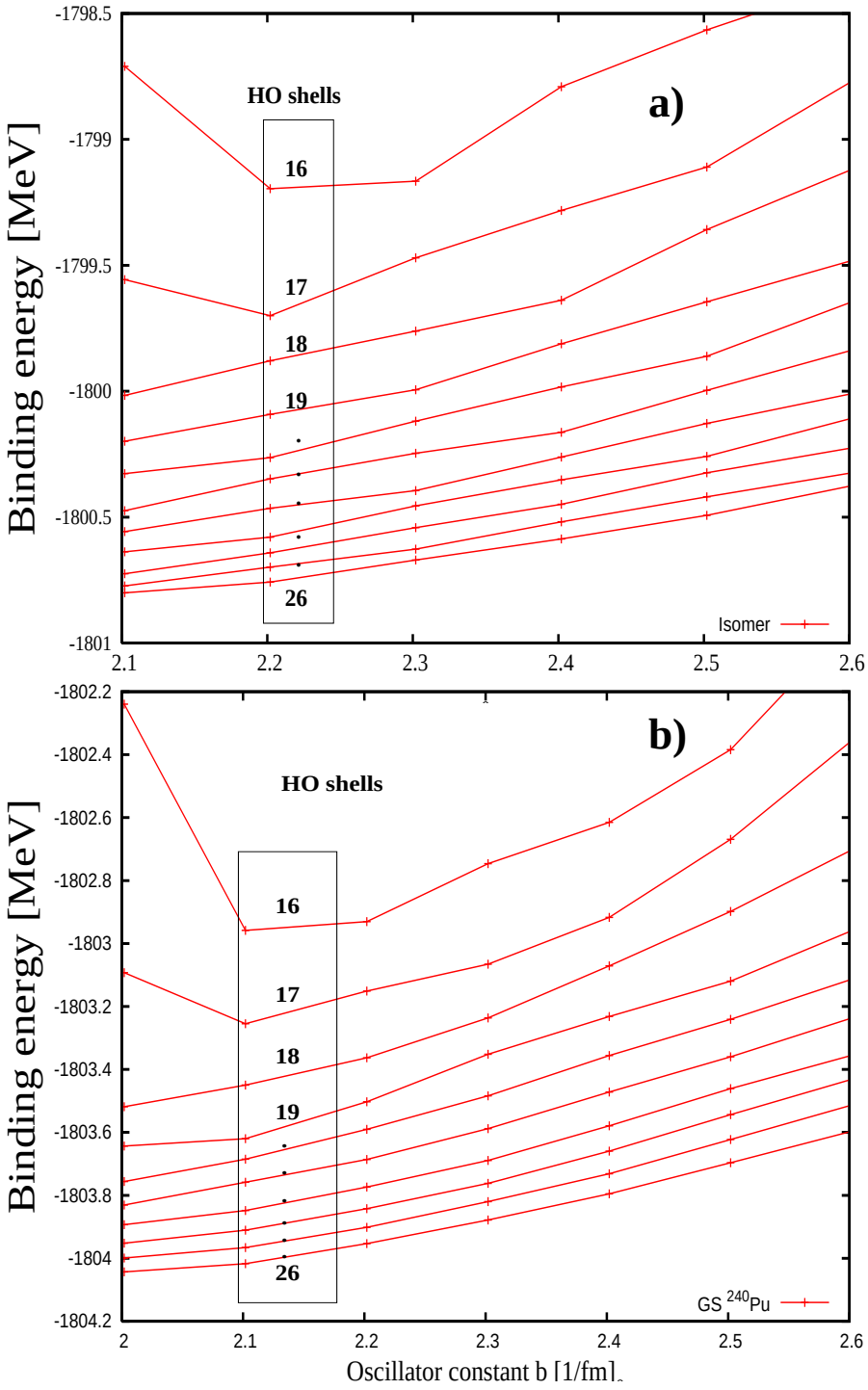

Figure 3.1: a) Optimization of the fission isomer binding energy in ^{240}Pu in the case of SkM* Skyrme interaction with respect to the oscillator constant $\sim b_\mu$ and the HO basis size done by HFBTHO Ref. [68]. b) Optimization of the ground state binding energy.

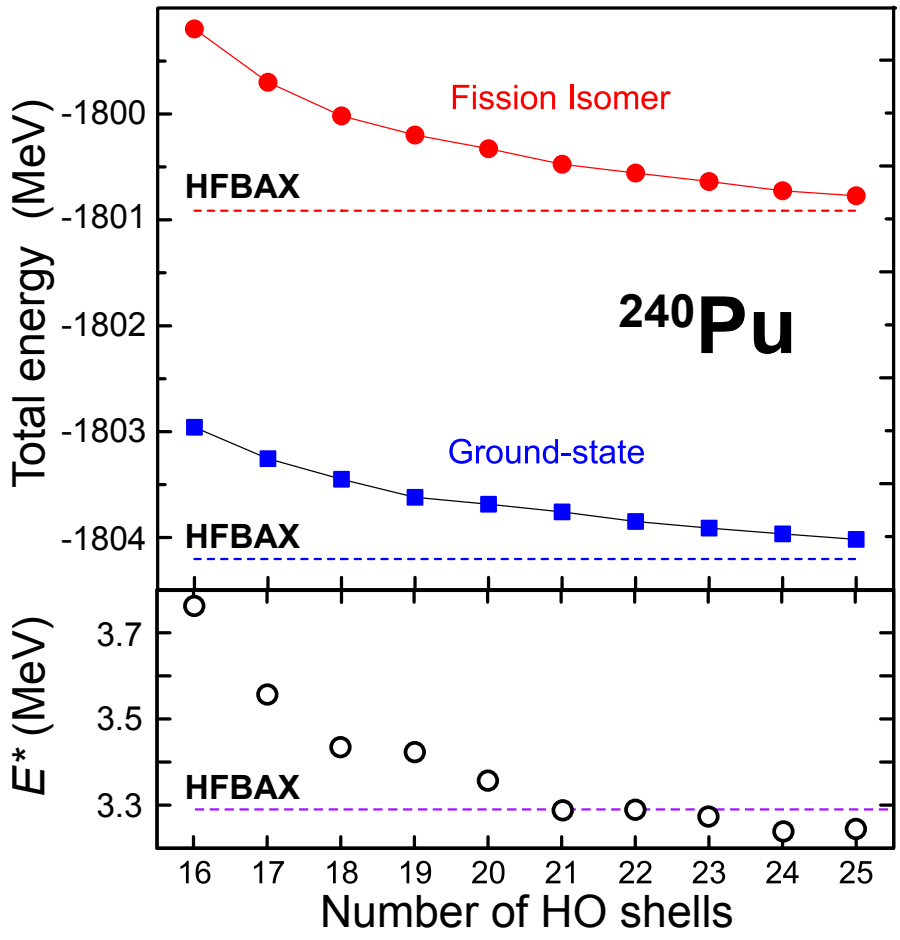

Figure 3.2: Convergence of the HO basis expansion for the HFB+SkM* binding energy of the fission isomer and ground state (top panel) and the excitation energy of fission isomer (bottom panel) in ^{240}Pu as a function of the HO basis size. Results are compared with the benchmark numbers obtained with the precise coordinate-space solver HFBAX Ref. [85].

3.2 Extraction of the smooth Liquid Drop using Strutinsky Theorem

3.2.1 Motivation

The focus of this research is to study LDM part of nuclear energy functionals in nuclei, by taking SD states as study cases. Therefore, a method of extraction of the Liquid Drop energy from the excitation energies of those states must be derived.

Within the framework of self-consistent calculations there are two methods for the extraction of the macroscopic energy: the Strutinsky shell correction method and the Thomas-Fermi + Wigner Kirkwood expansions. Strutinsky's method uses the single-particle energies to compute the shell correction by a smoothing polynomial function. The Thomas-Fermi + Wigner Kirkwood expansion method uses Thomas-Fermi equations and the gradient expansion of the partition function of the Hamiltonian. It was proven by Ref. [86] that both methods are equivalent. In the current research, Strutinsky's method is used in order to ensure that the results are consistent with Ref. [55], where the LDM parameters associated with Skyrme functionals used in this work were computed.

3.2.2 Strutinsky's Theorem

Strutinsky's energy theorem provides a link between the Hartree-Fock method and the microscopic-macroscopic models of nuclei. According to the Strutinsky theorem Ref. [95, 96], the total binding energy of nuclei is a sum of the macroscopic smooth energy E_{smooth} and the shell correction δE_{shell} rooted in the non-uniform discribtion of discrete single-particle levels,

$$E_{\text{HF}} = E_{\text{smooth}} + \delta E_{\text{shell}}. \tag{3.11}$$

The shell correction energy δE_{shell} can be calculated by the Strutinsky's renormalization procedure (method), which will be explained in the next two sections. Equation (3.11) represents the first order shell correction energy in the density variation. The most general expression of Strutinsky theorem also considers higher order shell correction Ref. [93]. It has been shown that the higher order shell corrections for heavy nuclei are ~ 1.5 MeV, and they weakly change with particle number or deformation. Due to the fact that the

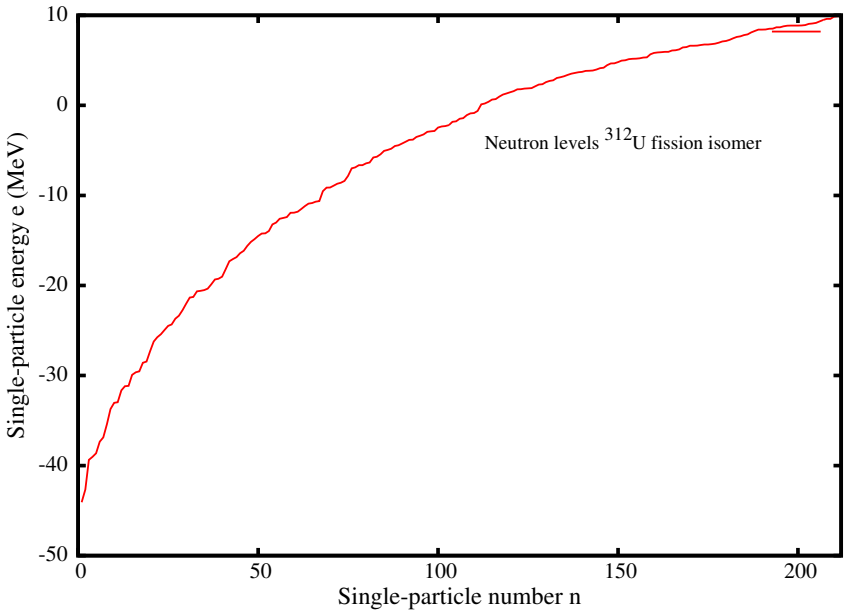

Figure 3.3: Demonstration plot of the neutron single-particle ϵ (e on the plot) energy in ^{312}U fission isomer as a function of the single-particle number n. ϵ is same as ϵ^{stair} from (3.12).

current research considers excitation energies in heavy nuclei (such as the actinides), these higher order shell corrections are expected to be of minor importance. Consequently, they are neglected in this work.

3.2.3 Strutinsky's renormalization procedure

Figure 3.3 shows neutron single-particle levels $\epsilon_{s.p.}(n)$ as a function of single-particle number n. As one can see, there is an overall global increasing trend, but also local fluctuations around this average trend. The line also defines the border of an area given by the integral of single-particle energy with respect to n: Since $\epsilon_{s.p.}(n)$ is discrete, one can replace this integral by a sum over n. This gives an estimate of the total single-particle energy. One can now find the smooth monotonous function that best reproduces the global smooth trend and calculate the corresponding area from it. The difference between these two integrals, using the discrete $\epsilon_{s.p.}(n)$ and continuous smooth function, gives the shell correction energy δE_{shell}:

$$\delta E_{shell} = \sum_{i=1}^{n} \epsilon_i - \int_0^N \bar{\epsilon}(n) dn. \tag{3.12}$$

The particle number N defines the Fermi level λ. Noting $dn(\epsilon)$, the number of states between ϵ and $\epsilon + d\epsilon$, one can write:

$$n(\epsilon) = \int_{-\infty}^{\lambda} dn(\epsilon) = \int_{-\infty}^{\lambda} \frac{dn(\epsilon')}{d\epsilon'} d\epsilon' = \int_{-\infty}^{\lambda} g(\epsilon') d\epsilon' = \int_{-\infty}^{\lambda} \sum_{i=1}^{\infty} \delta(\epsilon' - \epsilon_i) d\epsilon'. \tag{3.13}$$

The level density $g(\epsilon)$ can also be decomposed as the sum of a smooth part $\bar{g}(\epsilon)$ and a fluctuating part $\delta g(\epsilon)$ with respect to n (Figure 3.3). The smooth part $\bar{g}(\epsilon)$ is obtained by folding $g(\epsilon)$ by a smoothing function $f(x)$:

$$\bar{g}(\epsilon) = \frac{1}{\gamma} \int_{-\infty}^{+\infty} d\epsilon' g(\epsilon') f\left(\frac{\epsilon' - \epsilon}{\gamma}\right). \tag{3.14}$$

Usually the smoothing function $f(x)$ is represented by a Laguerre Polynomial $P(x)$ as $f(x) = P(x)\omega(x)$, where $\omega(x)$ is the Gaussian weighting and $\gamma \sim [\hbar\omega_0] = 41/A^{1/3}[MeV]$:

$$\omega(x) = \frac{1}{\sqrt{\pi}} e^{-x^2} \tag{3.15}$$

The Gaussian weighting $\omega(x)$ has been used for some time within Strutinsky's method. Other choices are also possible Ref. [102]. By using (3.14), the smoothed energy can be calculated as:

$$E_{smooth} = \int_{-\infty}^{\lambda_{smooth}} \epsilon \bar{g}(\epsilon) d\epsilon, \tag{3.16}$$

where λ_{smooth} is the Fermi energy corresponding to the smooth density, which is obtained by the condition on the particle number N

$$N = \int_{-\infty}^{\lambda_{smooth}} \bar{g}(\epsilon) d\epsilon \tag{3.17}$$

The values of γ and the order p of the Laguerre Polynomial should be chosen to satisfy the *plateau condition* for the smoothed energy E_{smooth}:

$$\begin{aligned} \frac{\partial E_{smooth}(\gamma, p)}{\partial \gamma} &= 0 \\ \frac{\Delta E_{smooth}(\gamma, p)}{\Delta p} &= 0 \end{aligned} \tag{3.18}$$

Typically $\gamma = 1.2 \times [\hbar\omega_0]$ and $p = 6$.

3.2.4 Continuum Effects and the Generalized Strutinsky Method

What has been shown so far does not include the contribution of positive continuum energy levels, which give spurious contributions to the shell correction. Therefore, the standard Strutinsky expressions have to be modified to remove this unwanted component. The practical method was developed by Ref. [102]. The level density $g(\epsilon)$ can be written as:

$$g(\epsilon) = -\frac{1}{\pi} Im\{Tr\left[\hat{G}^{\dagger}(\epsilon) - \hat{G}^{\dagger}_{free}(\epsilon)\right]\}, \tag{3.19}$$

where $\hat{G}^{\dagger}(\epsilon)$ is the single-particle Green's function and $\hat{G}^{\dagger}_{free}(\epsilon)$ is the Green function of the free gas. One can show Ref. [102] that

$$g(\epsilon) \approx \sum_{i=1}^{\infty} \delta(\epsilon - \epsilon_n) - \sum_{i=1}^{\infty} \delta(\epsilon - \epsilon_n^{free}), \tag{3.20}$$

This s.p. density renormalization for the non-resonant continuum contribution has to be used in (3.14). Such gerenarlization method for calculating shell corrections was implemented in this case by adding the contribution of the free Fermi gas into a shell correction code based on Ref. [105]. In practice it was done as follows:

- Diagonalization of the kinetic energy for neutrons and the kinetic + Coulomb energy for protons yields a set of discrete positive energy eigenstates. To this end, a procedure was implemented in HFODD by using an HO basis mesh.

- With free gas positive eigenstates, one can construct the level density $g^{free}(\epsilon)$ and apply (3.16)-(3.17) to compute the contribution to the shell correction δE_{shell} due to the free Fermi gas. This was done both for protons and neutrons after the self-consistent solution had been reached.

- Finally, several test calculation have been carried out to study the *plateau condition* and convergence behavior of the obtained shell corrections.

3.2.5 Tests of the Generalized Plateau Condition

The analysis of the generalized plateau condition and the dependence of the shell correction on the size of the HO basis are important for the final extraction of the smooth excitation energy. Calculated shell effects usually depend on the size of the HO basis. When calculating the smooth excitation energy of a nucleus, the unsatisfied plateau condition and the basis dependence create a noise, which may pollute final results. Therefore, a careful analysis of sensitivity of $\delta E_{\mathbf{shell}}$ on model assumptions is in order.

The tests were carried out for two nuclei from the actinide region, ^{236}U and ^{240}Pu, and two parametrizations of the Skyrme interaction-based EDF, SLy4 and SkM*. Figure 3.4 presents the behavior of the smoothed level density $\bar{g}(\epsilon)$ as a function of the single-particle energy in ^{236}U at the equilibrum deformation of the fission isomer. The calculation was done with SLy4 HF and the smooth parameters γ from Ref. [102].

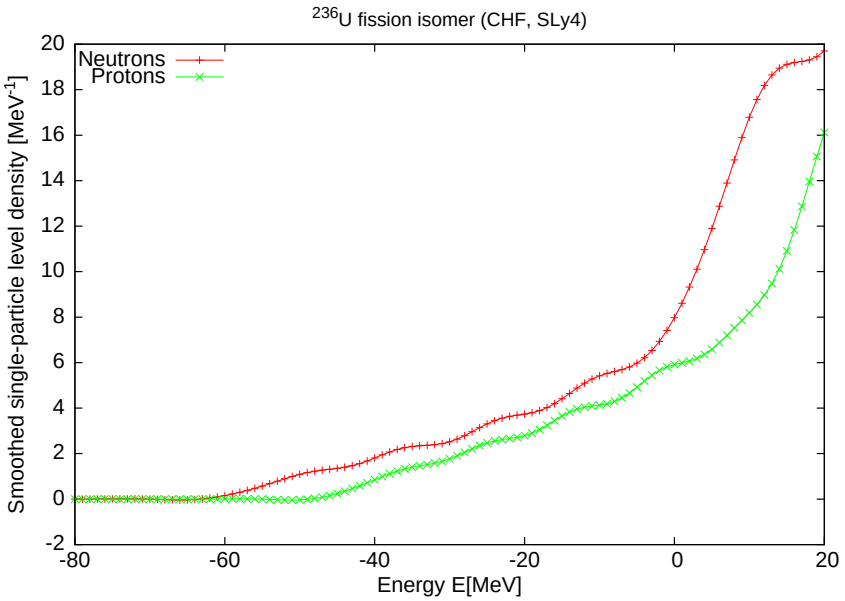

Figure 3.4: Illustration of the generalized $\bar{g}(\epsilon)$ for ^{236}U fission isomer, obtained in SLy4-CHF. The Strutinsky smoothing parameters are $\gamma_p = 1.54\times\hbar\omega_0$ for protons, $\gamma_n = 1.66\times\hbar\omega_0$ for neutrons, and $p = 10$.

Instead of HF, the HFB procedure with very small pairing gap has been used due to a technical problem: the HF convergence is usually more difficult to obtain, as it can have a "ping-pong" divergence (oscillating numerical solution between two numbers) due to the fixed single-particle occupation numbers and the crossing between different configurations. In the HFB case, this technical problem does not exist because of the quasi-particle concept of the HFB method, which ensures a smooth occupation of s.p. states. However, HFB calculations with sufficiently small pairing usually converge to HF. The HF solution can be obtained easily, but one has to ensure that pairing energy is very small at the end of the HFB convergence, by checking the occupation numbers of the quasi-particle states. If the occupation numbers converge to ~ 0 and ~ 1, then it is an HFB that gives an HF solution. If the occupation numbers are still between 0 and 1, then the HF solution is roughly approximated and it is necessary to re-run HFB with even smaller pairing.

An example of HF calculation is presented on Figure 3.4. There are small "ripples" in the proton case, which can be explained as an effect of the Coulomb barrier, according to Ref. [102]. The results shown on Figure 3.4 are practically independent of the choice of

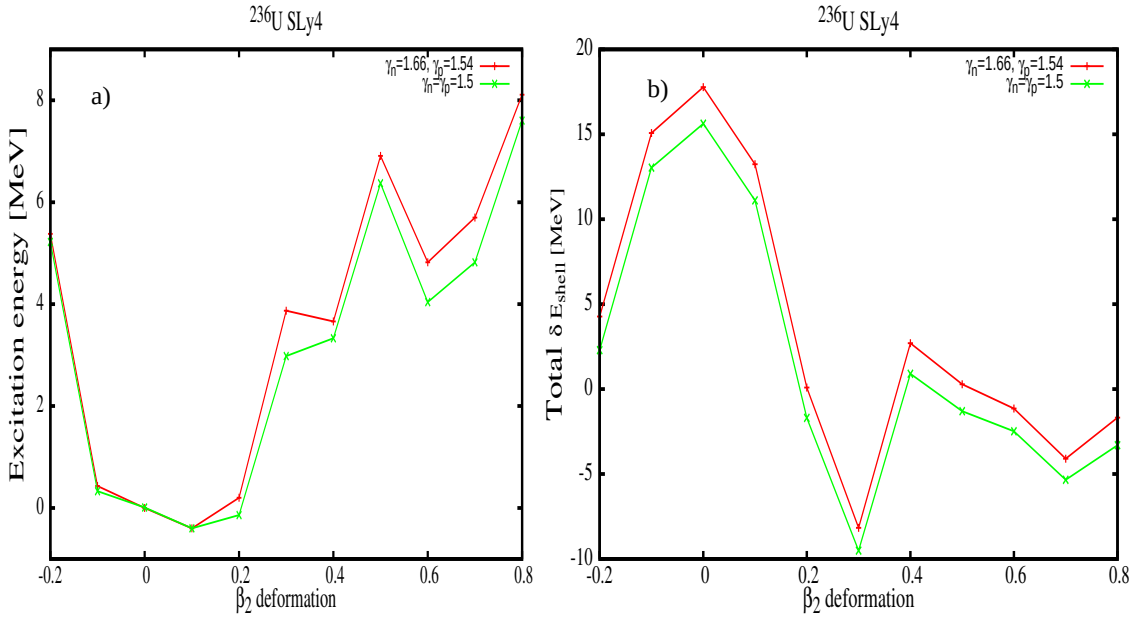

Figure 3.5: a) Potential energy surface of the smooth energy $E_{CHF} - \delta E_{shell}$, obtained with SLy4 Skyrme interaction and two different γ parameter sets; b) is the same as a), but shows the shell-corrections δE_{shell} at each deformation.

order p of Laguerre polynomials. Another test was done for the same nucleus, but in the case of SLy4-CHF within a wider region of β_2 constraints. The results are shown in Figure 3.5, which shows that the change of $\gamma_p = \gamma_n = 1.5$ to $\gamma_p = 1.54$ and $\gamma_n = 1.66$ creates ≈ 1 MeV shift of the whole smooth energy, as well as a small shift of δE_{shell}.

The second test was done for ^{240}Pu, both for the ground state and fission isomer. This test illustrates the convergence of the shell correction with respect to the HO size. It is based on the realistic minima from the unconstrained HFB calculations of Figure 3.2. Figure 3.6 plots the shell correction residual $\delta E^{SD}_{shell} - \delta E^{GS}_{shell}$ with respect to the number of HO shells in the basis. The shell correction residual exhibits a fluctuation within a 200 keV energy range, which is ~ 20 times smaller than the conclusive results presented in Chapters 4 and 5.

The performed tests show that with the current parameters and technique the generalized plateau conditions are satisfied and the fluctuations of the shell corrections are rather small with respect to the size of the HO basis.

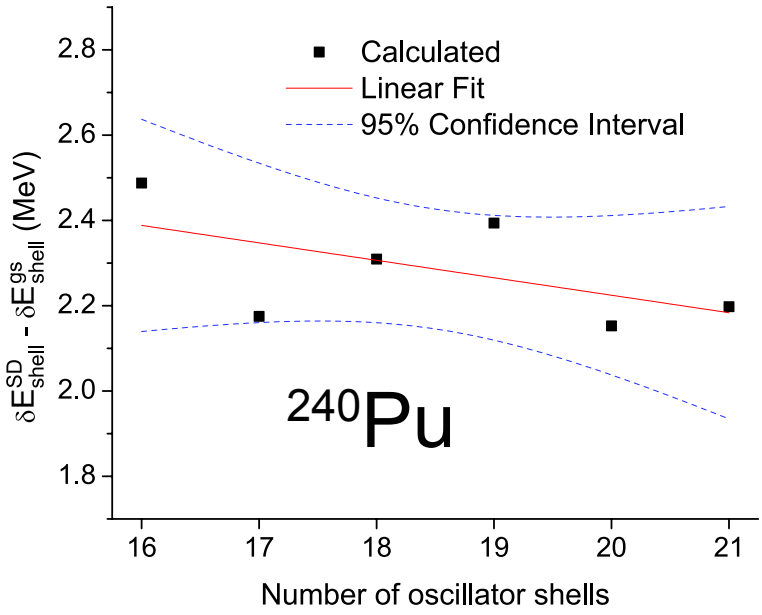

Figure 3.6: Convergence of the shell correction contribution to the deformation energy, $\delta E^{SD}_{shell} - \delta E^{GS}_{shell}$, for ^{240}Pu as a function of N_{max}. Calculations were performed with SkM* EDF.

3.3 Constrained Hartree-Fock and Potential Energy surfaces

3.3.1 Quadratic Constraint

In the current research, the LDM excitation energy of SD from HFB results has to be extracted. This is done in two steps. First, HFB calculations are performed for both the ground and SD state. These calculations yield the actual equilibrium deformations. Second, constrained HF calculations must be carried out, free from pairing at the same equilibrium deformations. This is essential because the shell correction method must be applied to a well-defined set of single-particle states. Indeed the HFB theory, deals with quasi-particle states, and the concept of s.p. states is ill-defined there.

In the self-consistent HF/HFB approach, nuclei do not have *a priori*-defined geometrical shape. Instead, the geometry of the nucleus is controlled by expectation values of multipole operators, which depend self-consistently on the nucleonic density at the equilibrium. The multipole moments are constrained within the HF/HFB procedure as constraints and then the energy is minimized at the desired shape. Thus, one can know what the HF/HFB

energy is for that choice of multipole moments, i.e. shapes. The relation between deformations and multipole moments is explained in the following section. The current section displays how constraints on the multipole operators are used in the HF/HFB theory, and how the corresponding constrained energy is calculated. Both methods are based on the minimization of the energy by adding a Lagrangian function. The most simple version of the method is the linear Lagrangian function. Mathematically, it is defined as

$$\text{Problem} := \begin{cases} min_{\mathbf{x}} E(\mathbf{x}) \\ \text{subject to } g_i(\mathbf{x}) = 0 \qquad \text{i=1,2,...,m} \end{cases}$$

where $E : \mathbb{R}^n \to \mathbb{R}$ is an objective function (typically, the energy), $g_i : \mathbb{R}^n \to \mathbb{R}$ are the constraint functions, and the Lagrangian function $E^{'} : \mathbb{R}^{n+m} \to \mathbb{R}$ is given as

$$E^{'}(\mathbf{x}, \lambda) = E(\mathbf{x}, \lambda) + E_{mult}(\mathbf{x}, \lambda) = E(\mathbf{x}, \lambda) + \sum_{i=1}^{m} \lambda_i g_i(\mathbf{x}), \tag{3.21}$$

where $\lambda_i \in \mathbb{R}$ are the Lagrangian multipliers. Unfortunately, the linear constraint cannot access certain regions of the deformation energy surface [72]. This problem is solved by means of the quadratic constraint:

$$E^{'}(\mathbf{x}, \lambda) = E(\mathbf{x}, \lambda) + E_{mult}(\mathbf{x}, \lambda) = E(\mathbf{x}, \lambda) + \sum_{i=1}^{m} c_i (g_i(\mathbf{x}))^2, \tag{3.22}$$

where the Lagrange multipliers c_i are called stiffness factors. The constraints $g_i(\mathbf{x})$ are expressed in terms of expectation values of the multipole operators as:

$$E_{mult} = \sum_{\lambda\mu} C_{\lambda\mu} \left(\langle \hat{Q}_{\lambda\mu} \rangle - \bar{Q}_{\lambda\mu} \right)^2, \tag{3.23}$$

where $\langle \hat{Q}_{\lambda\mu} \rangle$ are the average multipole moments, $\bar{Q}_{\lambda\mu}$ are the requested values for the multipole moments and $C_{\lambda\mu}$ are the corresponding stiffness factors.

An example of calculations employing quadratic constraint is shown on Figure 3.7. It presents the Potential Energy Surface (PES) as function of axial quadrupole deformation β (definition in section 3.4) for two nuclei, ^{194}Pb and ^{236}U, obtained within the CHFB approach using six different Skyrme EDFs.

3.3.2 Augmented Lagrangian Method

This section presents more accurate version of the Lagrangian Method used in this thesis. It is known as the "Augmented Lagrangian Method" (ALM). It combines the quadratic penalty method with the linear Lagrange parameters. The function that is minimized in

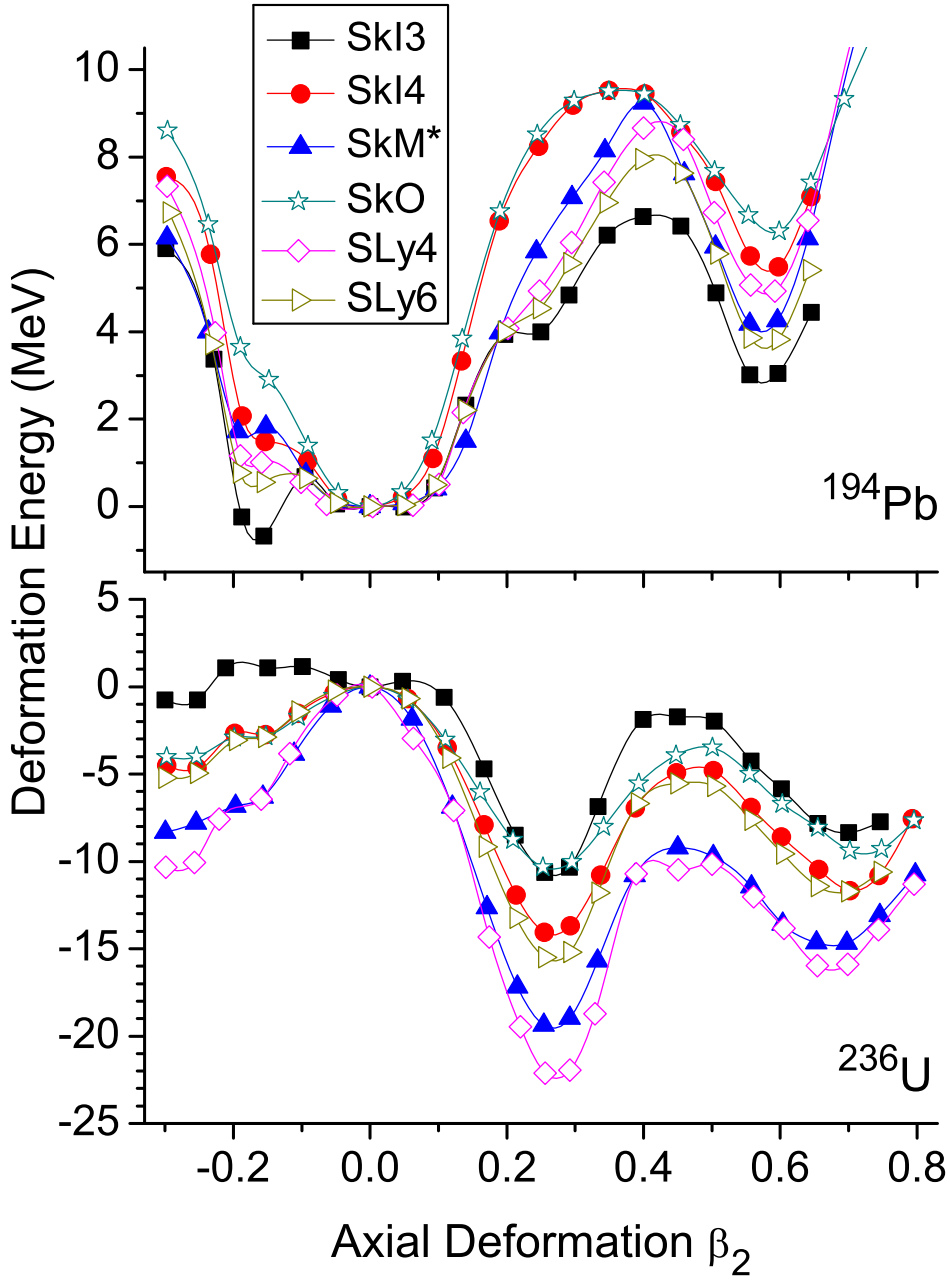

Figure 3.7: Potential Energy curves versus quadrupole deformation β (quadratic constraint with axial symmetry HFBTHO [68]) for ^{194}Pb and ^{236}U (see Table 4.1 and 4.2) obtained in HFB with different Skyrme interactions. The curves are normalized to the spherical point.

ALM is:

$$E_c^{'}(\mathbf{x},\lambda) = E(\mathbf{x},\lambda) + E_{mult}(\mathbf{x},\lambda) = E(\mathbf{x},\lambda) + \sum_{i=1}^{m}\lambda_i g_i(\mathbf{x}) + c\sum_{i=1}^{m}(g_i(\mathbf{x}))^2, \tag{3.24}$$

The Lagrange multipliers λ are modified iteratively by the relation [89]

$$\lambda^{k+1} = \lambda^k + 2cg\left(\mathbf{x}^k\right). \tag{3.25}$$

The ALM was implemented in the main HFB codes used in this thesis HFODD and HFBTHO [68, 71]. It was demonstrated in Ref. [89] that this method can give the desired multipole moment with arbitrary precision, which is very useful in the case of multi-constraint HF/HFB calculations, such as CHF calculations in the second minimum, or in large-scale applications like multi-modal fission study [89]. The only problem is that the ALM requires large CPU times to converge. Therefore, the methods described in Ref. [57] and Ref. [90] for multi-constraint HF/HFB calculations have also been used.

3.4 Multipole Moments and Bohr Deformations

This section presents the methods of extracting geometrical deformations from expectation values of HFB multipole moments.

The shape of the nuclear surface can be expanded in multipoles:

$$R(\theta,\phi) = R_0\left(1 + \sum_{\lambda=1}^{\infty}\sum_{\mu=-\lambda}^{\lambda}\alpha_{\lambda\mu}Y_{\lambda\mu}(\theta,\phi)\right). \tag{3.26}$$

In self-consistent calculations, the spherical radius R_0 and the deformation coefficients $\alpha_{\lambda\mu}$ can be obtained from the nucleonic density distribution ρ. Usually this is done by comparing the LDM multipole moments to the multipole moments obtained with the self-consistent density distribution.

Given the density ρ, one can construct the volume multipole moments $\bar{Q}_{00}^S$ and $\bar{Q}_{\lambda\mu}$ as average values, i.e.,

$$\bar{Q}_{\lambda\mu}^S = \int\int\int d^3\vec{r}\rho(\vec{r})r^2Y_{\lambda\mu}^* \tag{3.27}$$

$$\bar{Q}_{\lambda\mu} = \int\int\int d^3\vec{r}\rho(\vec{r})r^{\lambda}Y_{\lambda\mu}^*, \tag{3.28}$$

The monopole moments $\bar{Q}_{00}^S$ and $\bar{Q}_{00}$ are the root-mean-square radius and the total particle number, respectively.

Let one now assume a reference body with a uniform constant density ρ_0 and a geometrical shape parametrized by (3.26). The corresponding geometrical multipole moments are determined by the integrals

$$Q^S_{00}(\rho_0, R_0, \alpha) = \frac{\rho_0}{5} \int_0^{2\pi} d\phi \int_0^{\pi} \sin\theta d\theta R^5(\theta, \phi) \tag{3.29}$$

$$Q_{\lambda\mu}(\rho_0, R_0, \alpha) = \frac{\rho_0}{\lambda + 3} \int_0^{2\pi} d\phi \int_0^{\pi} \sin\theta d\theta R^{\lambda+3}(\theta, \phi) Y^*_{\lambda\mu}(\theta\phi). \tag{3.30}$$

When we combine (3.27)-(3.28) and (3.29)-(3.30), the resulting system of equations is Ref. [66, 67, 69, 70]:

$$Q^S_{00}(\rho_0, R_0, \alpha) = \bar{Q}^S_{00} \tag{3.31}$$

$$Q_{\lambda\mu}(\rho_0, R_0, \alpha) = \bar{Q}_{\lambda\mu}, \tag{3.32}$$

with the deformation parameters $\alpha_{\lambda\mu}$ as unkowns. This system of equations is solved iteratively. In the case of small deformations, (3.31)-(3.32) can be solved in the order around $\alpha_{\lambda\mu} = 0$:

$$\begin{aligned} \rho_0 &= \frac{3}{4\pi} \frac{\bar{Q}_{00}}{R_0^3}, \\ R_0 &= \sqrt{\frac{5}{3}} \bar{R}_{rms}, \\ \alpha_{\lambda\mu} &= \frac{4\pi}{3a_{\lambda\mu}} \frac{\bar{Q}_{\lambda\mu}}{\bar{Q}_{00} R_0^{\lambda}} \end{aligned} \tag{3.33}$$

Equations (3.31)-(3.32) are usually solved numerically. This is done in two steps: computing the integrals (3.27)-(3.28) and (3.29)-(3.30) with the Gauss-Legendre quadrature, and then solving (3.31)-(3.32) iteratively. The final values of the deformations depend on the maximum multipolarity λ_{max} in (3.26). To guarantee good convergences one usually takes $\lambda_{max} = \lambda + 2$, where λ is the maximum multipolarity of the multipole moments that are considered as constraints.

In HFODD, the final deformations $\beta_{\lambda\mu}$ are calculated from the resulting coefficients $\alpha_{\lambda\mu}$ as

$$\beta_{\lambda\mu} = \alpha_{\lambda\mu} \sqrt{2 - \delta_{\mu 0}}. \tag{3.34}$$

The extraction of the liquid drop surface deformations needed in the current research is discussed in the next section.

3.5 Computing the Surface Moments, Charge Radii, and LDM Deformations from HFB Density

3.5.1 Surface Moments, Development of the "SMOMENTS" Routine

In the two previous sections it was illustrated how, within HFB, one can define nuclear shape by using expectation values of the multipole moment operators, and then calculate the first order and exact Bohr shape deformations of a shape by solving a system of non-linear equations.

The LDM deformations can not be reliably computed from the volume multipole moments (3.29), but should rather be obtained from the surface moments (3.28). This is because the volume multipole moments artificially exaggerrate the role of the higher-order multipoles [73]. In this work, a new routine called "SMOMENTS" has been developed, which uses HFODD densities as an input. In our work only axial-shapes, $Y^*_{\lambda\mu}(\theta,\phi) = Y_{\lambda 0}(\theta,\phi)$ are considered. In particular, the surface quadrupole moment written in Cartesian coordinates is

$$\bar{Q}^S_{20} = \sqrt{\frac{5}{4\pi}} \int\int\int d^3\vec{r}\rho(\vec{r})r^2(2z^2 - x^2 - y^2). \tag{3.35}$$

Numerically, the 3-fold integral (3.35) are solved by Gauss-Hermite quadratures. The weights w_l, the density ρ and the exponential factors $e^{-\frac{\xi^2_\mu}{2}}$ are taken from the output file of HFODD. The input for "SMOMENTS" also contains the current number of shells N_{shell} and the oscillator constants b_μ, as they are defined in HFODD. The code "SMOMENTS" was developed in two steps. First, the code calculates the proton, neutron, and particle numbers by a simple integration for $\lambda = 0$. This first step verifies that the code uses the correct density, number of shells N, and oscillator constants b_μ. If the code produces the correct proton and neutron numbers, then the second step calculates all axial ($\mu = 0$) surface moments up to $\lambda = 8$.

Included below is an example of the "SMOMENTS" output in the particular case of ^{236}U fission isomer with SkI4 Skyrme functional. The code calculates also the multipole moments (3.28) as they are in HFODD, as an additional validation.

Nx = 42 Ny = 42 Nz = 60 Mx = 42 My = 42 Mz = 60

ATOMIC NUMBER: 236.000009538093

==========

SURFACE MOMENTS FOR LAMBDA=0,2,4,6,8

==========

Q(0,0): 96.6426754702382 x100

Q(2,0): 87.1085233061156 x100

Q(4,0): 12.2088684511216 x100

Q(6,0): 4.96006172411692 x100

Q(8,0): 1.49763055418450 x100

==========

VOLUME MULTIPOLE MOMENTS FOR LAMBDA=4,6,8

==========

Q(4,0): 11.7287221913591 x10E+4

Q(6,0): 5.97175124256956 x10E+6

Q(8,0): 3.05638240940431 x10E+8

==========

READING HFODD REC FILE, ALL RIGHT

In the case of 20 shells, M=42 quanta in every direction for spherical shapes have been used. In the case of highly deformed fission isomer, $M_z = 60$ quanta in z-direction in order to ensure convergence of the intergration.

3.5.2 Linking HFB/CHF Surface Moments to LDM Deformation Parameters

This section presents the method of extraction of the LDM deformation parameters from the calculated HFB/CHF surface moments (3.35). The transformation is given by the set of equations Ref. [73]:

$$\left.\frac{Q_\lambda^S}{Q_0^S}\right|_{HF} = \left.\frac{\langle r^2 Y_{\lambda 0}\rangle}{\langle r^2\rangle}\right|_{HF} = \left.\frac{Q_\lambda(\tilde{\beta}_\lambda)}{\langle r^2\rangle}\right|_{LDM}, (\lambda = 2, 4, ...\lambda_{max}), \tag{3.36}$$

where Q_λ^S and Q_0^S are respectively the surface multipole moments and the root-mean-square radius. The geometrical surface multipole moments of LDM depend on the (unknown)

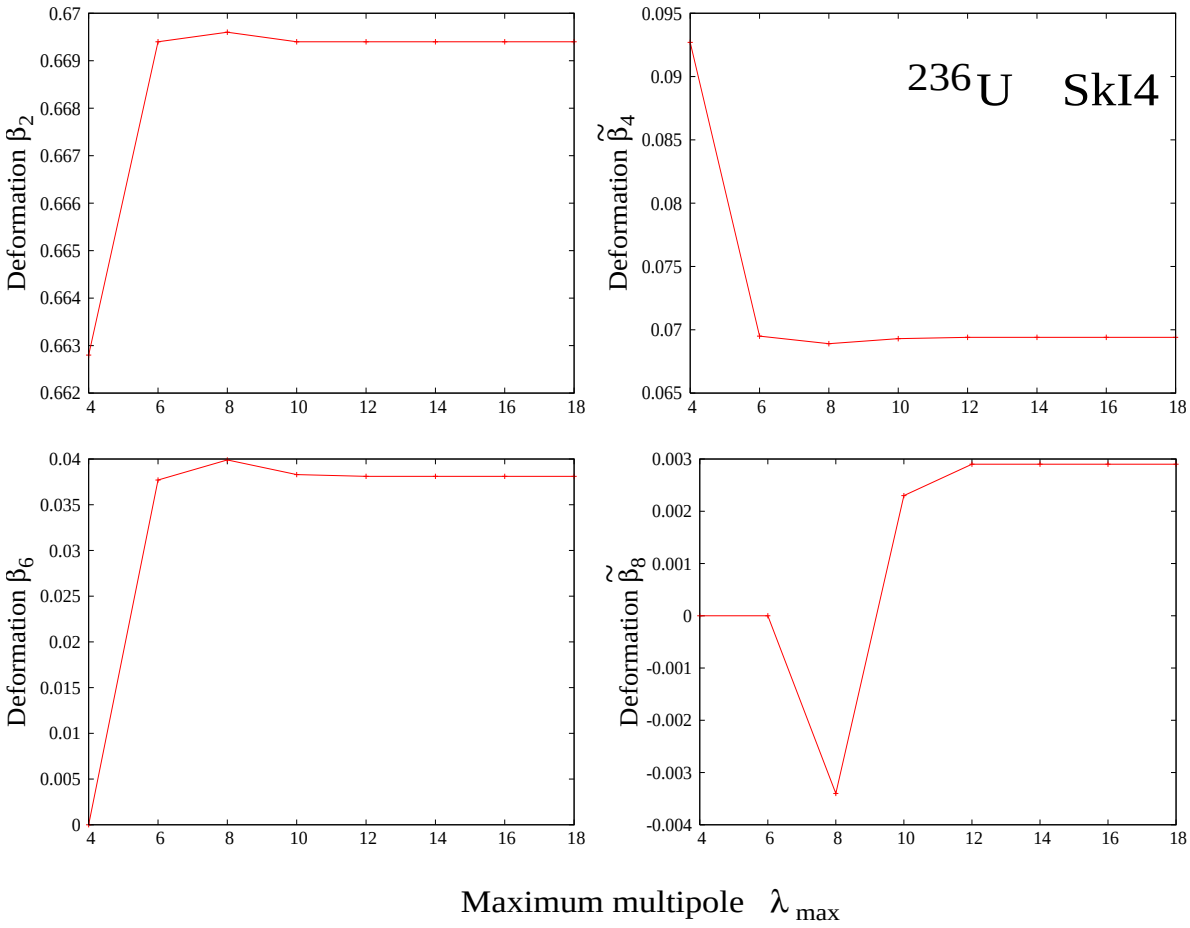

Figure 3.8: Deformation parameters $\tilde{\beta}_{2,4,6,8}$ of a ^{236}U fission isomer obtained by solving (3.38) for different values λ_{max}. HFB calculations were carried out with SkI4 EDF.

deformations $\tilde{\beta}_{\lambda 0}$. Equations (3.36) are independent of the overall scaling factors r_0. The system of equations (3.36) is solved for λ_{max} large enough to guarantee convergence. An example is shown on Figure 3.8, where $\lambda_{max} = 18$ is well enough to assume the saturation of the surface $\tilde{\beta}_2$ to $\tilde{\beta}_8$.

Once the deformation parameters $\tilde{\beta}_\lambda$ of the nuclear surface have been determined (3.26), one can obtain the geometrical form-factors $b_{\mathbf{surf}}$, $b_{\mathbf{curv}}$, $b_{\mathbf{Coul}}$ mentioned in Section 2.2.3 (see Ref. [72] and Ref. [74]). For the computation of $b_{\mathbf{surf}}$, $b_{\mathbf{curv}}$, $b_{\mathbf{Coul}}$ (Eq.(2.12)), a separate code developed in Ref. [79] has been used. The dependence of these coefficients on shape elongation $\tilde{\beta}_2$ is shown in Figure 3.9. In this example we consider only axial

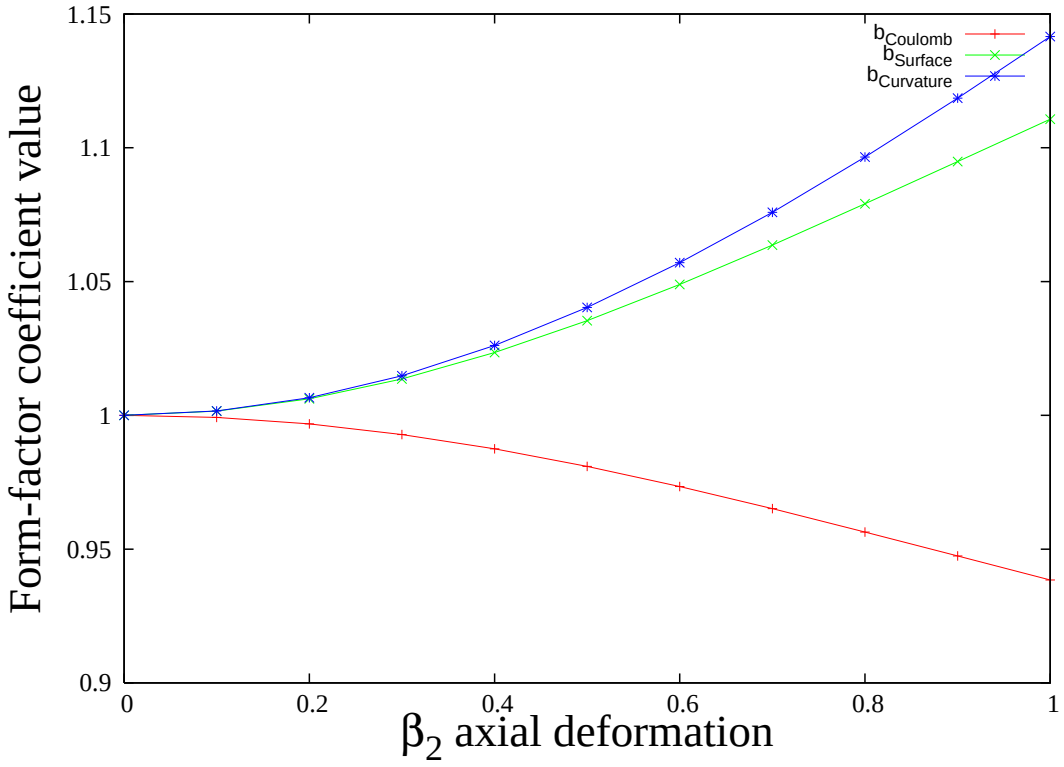

Figure 3.9: Coulomb, surface, and curvature geometrical form-factors a function of the axial quadrupole deformation $\tilde{\beta}_2$.

quadrupole moments. In the case of spherical shape, all coefficients b are of course equal to one.

A realistic example of how the shell energy was computed and how the equivalent LDM deformations were extracted is given on Figure 3.10, which presents the shell energy δR_{shell}, the extracted smooth deformation energy from $\tilde{E}_{\rm def}^{\rm HF}(\beta)$, and the corresponding LDM deformation energy $E_{\rm def}^{\rm LDM}(\beta)$ computed using deformations (3.36). Since the HF deformation energy is affected by configurations crossing (the sharp change in $\tilde{\beta}_4$ in the inset), the curves were not interpolated. However, the smooth deformation energy increases on the average with the deformation and agrees rather well with the extracted LDM deformation energy.

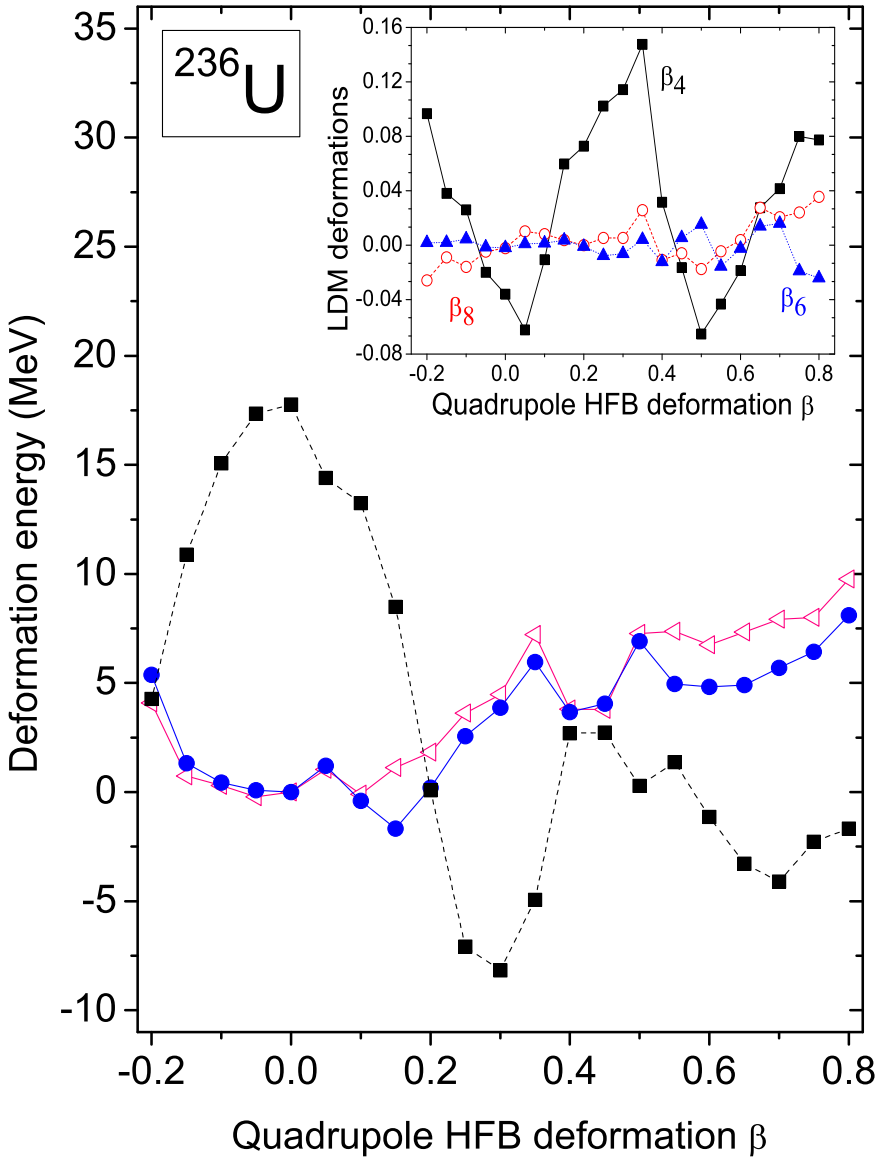

Figure 3.10: Extraction of the LDM deformation energy from constrained HF+SLy4 calculations for ^{236}U at several values of quadrupole deformation β. Shown are: the total shell correction $\delta E_{\rm shell}$ (squares), smooth HFB deformation energy $\tilde{E}^{\rm HF}_{\rm def}(\beta)$ (dots), and the corresponding LDM deformation energy $E^{\rm LDM}_{\rm def}(\beta)$ (triangles). The inset shows the equivalent LDM deformations $\beta_\lambda \equiv \tilde{\beta}_\lambda$ with λ=4,6, and 8

3.5.3 Calculation of the Coulomb Polarization Effect and Charge radii

As previously mentioned in Section 2.3, the LDM mass formula involves Coulomb energy, which depends on the spherical charge radii r_0^{ch}. In the case of realistic nuclei, the equilibrium deformations and shell energies are affected by the long-range Coulomb polarization (due to the mean field), but the LDM parameters of Ref. [55] used in that work were obtained without considering the Coulomb term. To resolve this inconsistency, r_0^{ch} has been extracted from the Hartree-Fock mean-field using the condition $(r_{ch}^2)^{HF} = (r_{ch}^2)^{LDM}$. Charge radius is directly related to the charge distribution form-factors Ref. [80, 132] and the neutron excess Ref. [84]:

$$\langle r_{ch}^2 \rangle = \langle r_p^2 \rangle + \langle r_{ch}^2 \rangle_p + \frac{N}{Z} \langle r_{ch}^2 \rangle_n, \tag{3.37}$$

where $\langle r_p^2 \rangle$ is the proton mean-square radius, $\langle r_{ch}^2 \rangle_p = 0.743[fm^2]$, and $\langle r_{ch}^2 \rangle_n = -0.119[fm^2]$. The mean-square radius of the proton distribution,

$$\langle r_p^2 \rangle = \int\int\int d^3\vec{r} \rho_p(\vec{r}) r^2, \tag{3.38}$$

has been obtained from HF calculations at the spherical shape. The equivalent LD radius was obtained using the usual relation:

$$r_0 = \sqrt{\frac{5}{3} \langle r_{ch}^2 \rangle} / A^{\frac{1}{3}}$$

Figure 3.10 for ^{236}U presents LDM results with the value of r_0 obtained in this way. Section 5.2 discusses an additional aspect of the Coulomb polarization related to the fissility of neutron-rich Uranium isotopes.

Chapter 4

Results

4.1 Deformation Energy of a Nuclear Liquid Drop

This section presents results of two LDM calculations performed using (2.13) for the cases of ^{100}Sn and ^{100}Zn. The main idea here is to highlight the contribution of the surface-symmetry energy to the total binding in neutron-rich heavy nuclei, and emphasize differences between different Skyrme EDFs. The nuclei considered in this example have the same mass A, but very different neutron excesses I.

First, one can consider the global trends of the volume symmetry, surface-symmetry and total symmetry energy for spherical nuclei with respect to their atomic mass A; the results are shown on Figure 4.1. The differences between various Skyrme EDFs for the volume and the surface symmetry energies are visible; they come from the differences of the corresponding LDM parameters listed in Table 5.1. However, the differences tend to be much smaller when it comes to the total symmetry energy.

The deformations used in ^{100}Sn and ^{100}Zn are fixed to β_2 =0.0 and 0.6, corresponding to spherical and super-deformed shapes, respectively. The Coulomb radius r_0 is taken to be the Wigner-Seitz radius defining the saturation density ρ_0. The results are shown in Figures 4.1 and 4.2.

In ^{100}Sn (Figure 4.2) one can see that for neutron excess $I = 0$, surface-symmetry energy is vanishes; hence, it does not contribute to the deformation energy. The LDM deformation energy hangs on the balance between surface and Coulomb terms. In the case

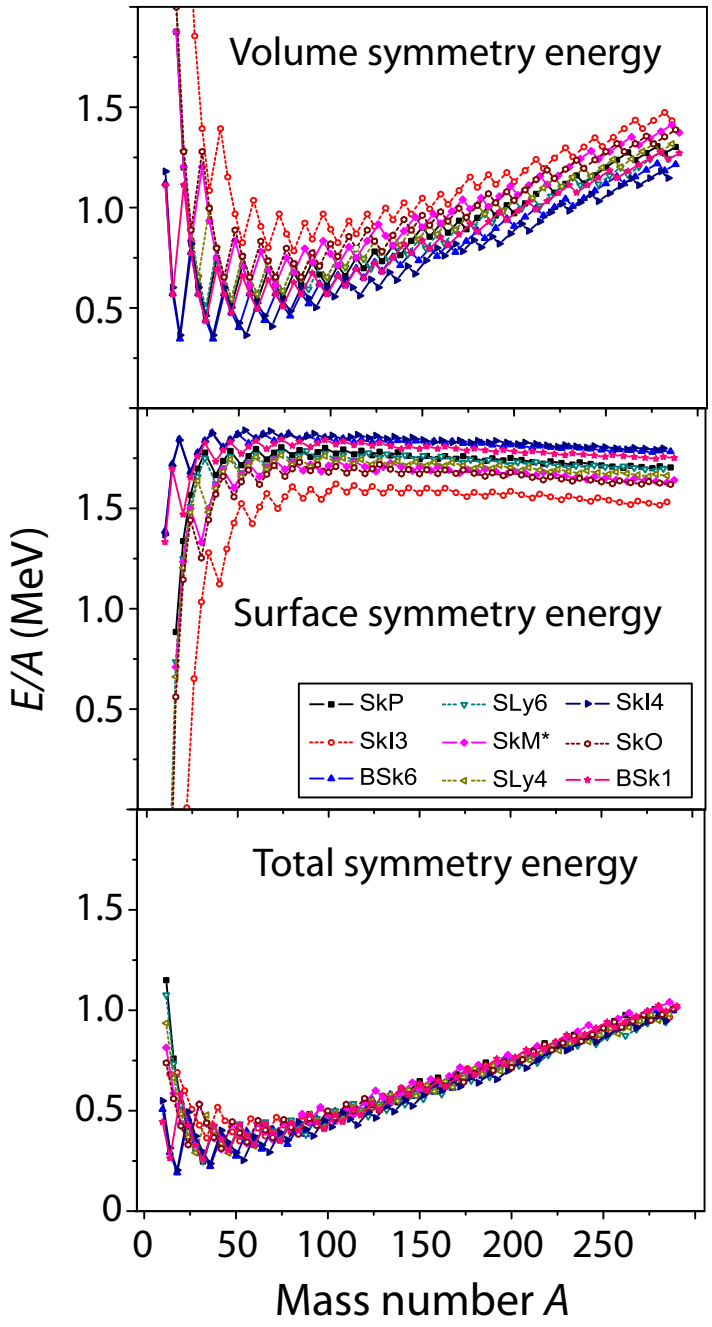

Figure 4.1: Contributions to the microscopic LDM energy per nucleon along the LDM valley of stability: volume symmetry term $a_{\rm sym}I^2$ (top), surface-symmetry term $a_{\rm ssym}I^2A^{-1/3}$ (middle), and the total symmetry energy (bottom), for the microscopic LDM derived from Skyrme EDFs of Table 2.2.

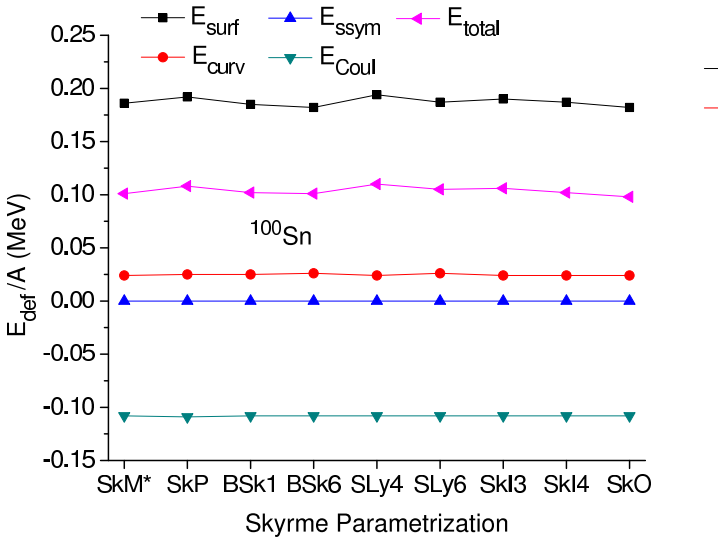

Figure 4.2: Total deformation energy of LDM for ^{100}Sn and its separate LDM components. β_2 =0.6 assumed.

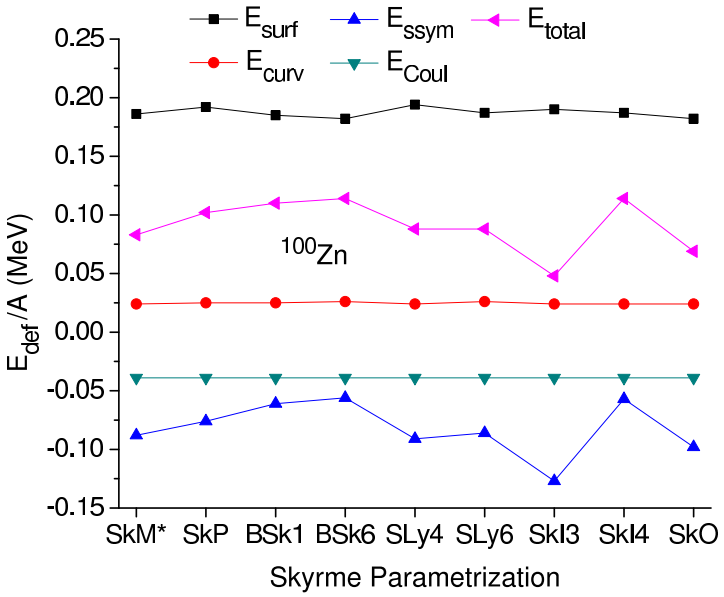

Figure 4.3: As in Fig.4.2 except for ^{100}Zn

of ^{100}Zn (Figure 4.3), the situation is rather different. The deformation energy is slowly impacted by the surface-symmetry energy. The large fluctuation of surface-symmetry energy between Skyrme EDFs results in uncertainties in deformation energies and this has important consequences for the fission of neutron-rich heavy nuclei. These results have led to three questions:

- Are the predicted excitation energies of highly-deformed configurations strongly sensitive to EDF parameters? This sensitivity might be related both to the shell energy and the LDM energy.
- What is the average deviation between experiment and theory for strongly deformed states for commonly used EDFs?
- Does the EDF surface-symmetry parameter $a_{\rm ssym}$ have a strong impact on the LDM deformation energy?

The answers to these questions are presented in the next section. In addition, Chapter 5 will show what happens when the HFB calculations are extended to extremely neutron-rich Uranium isotopes, where uncertainties in the LDM parameters become amplified by the neutron excess, and the surface-symmetry energy becomes crucial in deformed configurations.

4.2 HFB Results for Realistic Nuclei

Fission isomers are meta-stable SD configurations in the actinide nuclei. Their existence has been explained in terms of the shell effects beyond the inner fission barriers [64].

High-spin super deformation in heavy nuclei was observed for the first time experimentally around ^{152}Dy as a high-energy gamma-ray band structure Ref. [94]. It can be associated with the presence of a strongly elongated nuclear configuration. Several regions of nuclei with SD states have been discovered experimentally. These states are very useful in the study of the deformation properties of EDFs. Table 4.1 lists the experimental data used in this study.

Nucleus	$E_{SD}(0^+)$ (MeV)	Reference
^{192}Hg	5.3 (9)	[121]
^{194}Hg	6.017	[120]
^{192}Pb	4.011	[119]
^{194}Pb	4.643	[122]
^{196}Pb	5.630(5)	[124]
^{236}U	2.750	[118]
^{238}U	2.557	[118]
^{240}Pu	2.800	[118]
^{242}Cm	1.900	[118]

Table 4.1: Experimental energies of $I^\pi = 0^+$ bandheads of SD states in A=190 mass region and fission isomers in the actinides.

4.2.1 HFB Excitation Energy Results

This section discusses the HFB results for excitation energies and equilibrium deformations of SD states listed in Table 4.1. The purpose of these calculations is to demonstrate the significant uncertainty of the predicted excitation energies with respect to experiment, and to determine the impact of surface-symmetry energy. These calculations are also used to extract the equilibrium multipole moments from the ground state and SD states. All HFB calculations were performed in the space of 20 full oscillator shells, which results in a small (<200 keV) error on the deformation energy (see Figure 3.3).

The results of systematic calculations summarized in Figure 4.4, that shows the SD band-head energy residuals (experimental excitation energy - theoretical excitation energy). It can be immediately seen that for the selected EDFs there are ≈ 6-7 MeV fluctuations between the parametrizations and ≈ 3-4 MeV deviations from experiment. All these fluctuations and deviations from the experiment are much larger than the 200 keV theoretical error resulting from the size of the HO basis. In addition Figure 4.4 shows that some families of Skyrme EDFs yield very consistent results for both Hg-Pb nuclei and the actinides (such MSk1-6 and SkX(SkXC)). The differences between various EDFs are due to several factors. SLy[x] functionals, for example, treat the center of mass differently. BSk[x]

and MSk[x] EDF families are consistent with one another as they have been produced by the same group using the same optimization strategy.

The origin of large deviations from experiment seen in Figure 4.4 can be traced back to incorrect deformation parameters of commonly used EDFs. This does not come as a surprise because the standard fitting protocols do not include experimental data on fission barriers, isomers, and super-deformation. As mentioned earlier, exceptions are SkM* and BSk[x] EDFs.

To determine whether the deviations in Fig. 4.4 are caused by the surface-symmetry energy is a challenge as the shell effects obstruct the picture. Nevertheless, the qualitative fingerprints of the macroscopic surface energy can be seen on Figures 3.7 and 4.4. For instance, EDF functionals having low surface energy (see Table 2.2) yield soft PESs. More information can be extracted when the shell energy is removed. This is done in the next section.

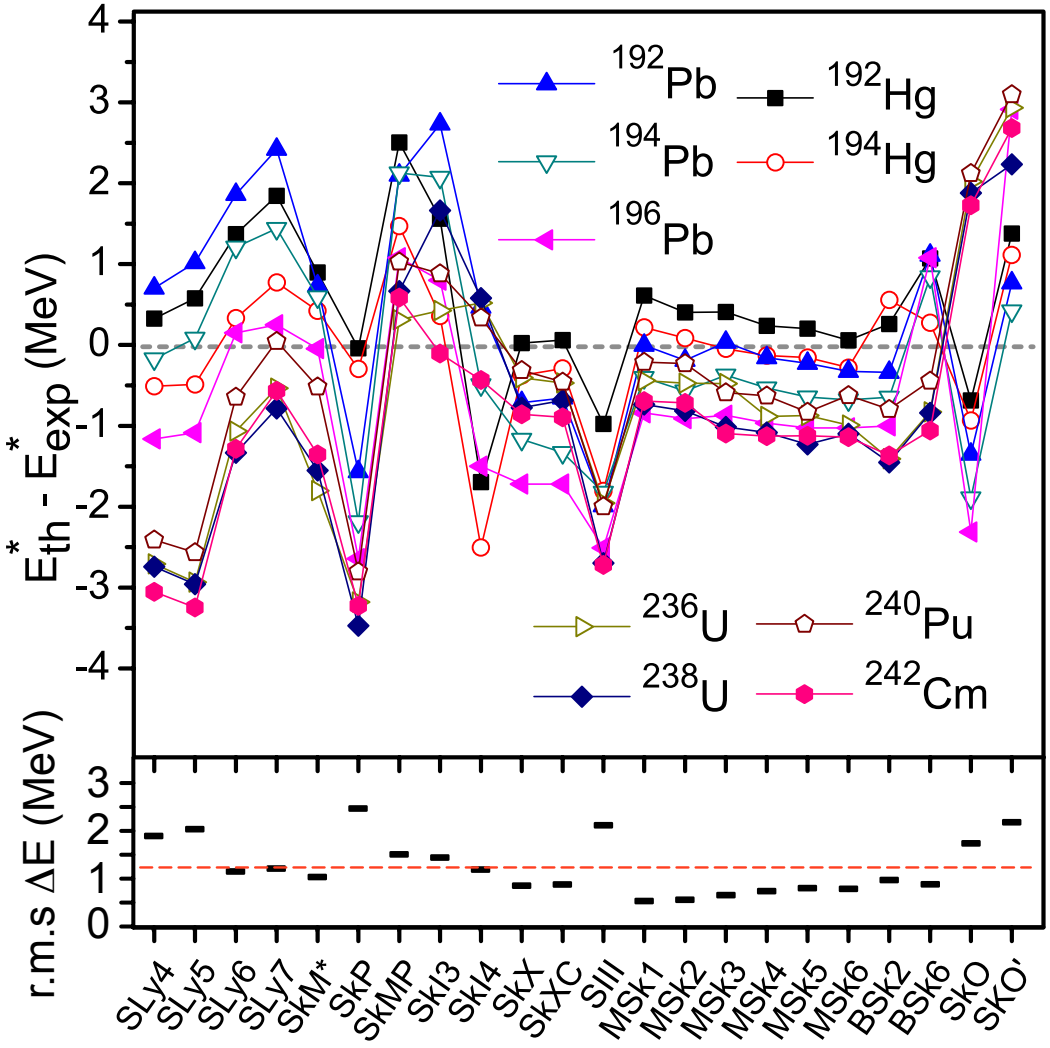

Figure 4.4: HFB residuals ($E^*_{th} - E^*_{exp}(MeV)$) from the excitation energy of super-deformed and fission isomers, calculated with various Skyrme force parametrizations (top panel) and the rms deviation from the experiment (bottom panel). The rms for all nuclei is 1.26 MeV (dashed line). MSk1 has the lowest rms, 0.53 MeV. SkI4 has the lowest rms for fission isomers, rms 0.48 MeV. References to EDFs: SLy4-7 [110], SkMP [98], SkX-SkXc [99], SIII [100], MSk1-6 [101], BSk2 [109], and SkO' [112].

4.2.2 Extraction of the smooth deformation energy of HFB

This section discusses the constrained HF calculations and the extraction of corresponding shell corrections. Figures 4.2 and 4.3 demonstrate that the uncertainties in $a_{\rm ssym}$ have a strong influence on the deformation properties of neutron-rich nuclear drops. Now it is interesting to see whether a similar uncertainty shows up in the HFB results as well.

Figure 4.5 shows the smooth excitation energy of fission isomers calculated in HFB and LDM for seven EDFs. For each nucleus, we carried out HFB calculations to determine the g.s. and SD configurations. The constrained HF calculations are then performed based on the multipole moments of the HFB solution. Shell energies are subtracted from g.s. and SD HF energies, and this defines the smooth part of the excitation energy EHFB in HFB, i.e., the smooth deformation energy of the excited state relative to the ground-state. Using the surface moments obtained in the g.s. and SD minima of HFB, we extract the equivalent LDM deformation parameters and the LDM excitation energy.

The results for the SD bandheads are displayed in Fig. 4.6. In these lighter nuclei, the agreement between HFB and equivalent LDM is better on the average, but local fluctuations can be appreciable (see SkO or SkI3 results for Pb isotopes) and might be related to a complex pattern of g.s. equilibrium deformations in these nuclei.

The clear differences between various EDF parameterizations can be seen. Overall, these variations can be as large as 4 MeV at the LDM level.

The results shown in Figs.4.5 and 4.6, combined with the overall picture of the residuals in Fig.4.4, demonstrate that large differences between Skyrme EDFs exist when it comes to deformation properties of nuclei. While these differences certainly depend on variations of EDF parameters controlling the shell structure, such as, e.g. the effective mass or spin-orbit splitting, our analysis indicates that there are also fundamental discrepancies at the level of the bulk energy. One may therefore question whether EDF optimization protocols based exclusively on a small amount of data on nuclear matter properties and spherical nuclei are able to capture the deformability of EDF.

Figure 4.7 shows the surface and surface symmetry contributions to the LDM excitation energy of SD states in the actinides for the same Skyrme EDFs as in Figs. 4.5 and 4.6. The equilibrium deformations that are used in the LDM for both the ground-state and SD

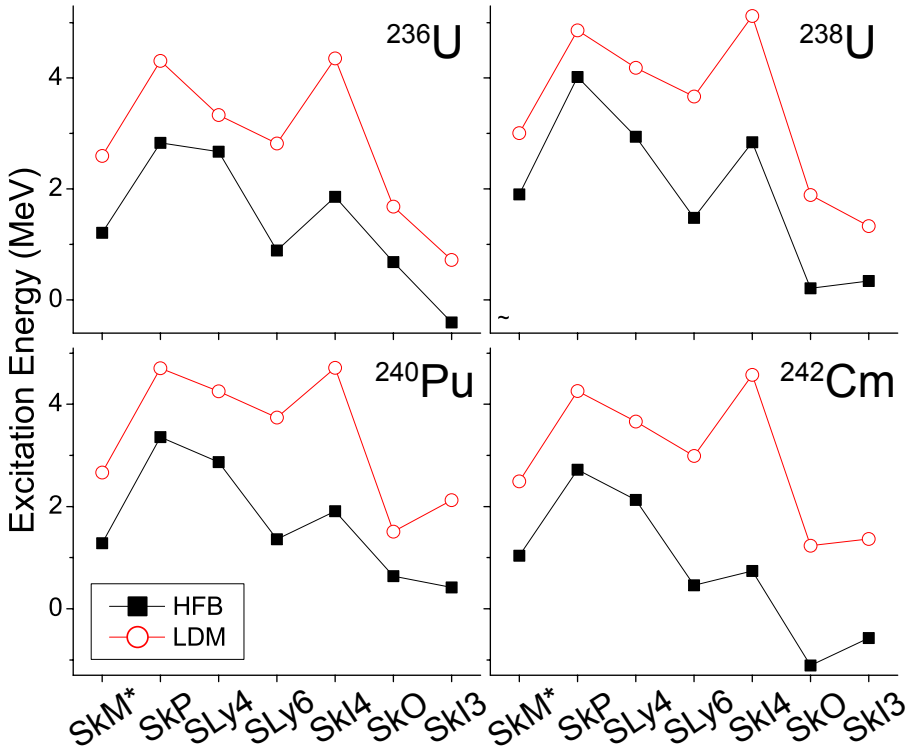

Figure 4.5: (color-online) Smooth excitation energy E* fission isomers in ^{236,238}U, ^{240} Pu, and ^{242} Cu calculated in HFB and LDM for seven EDFs. See text for details.

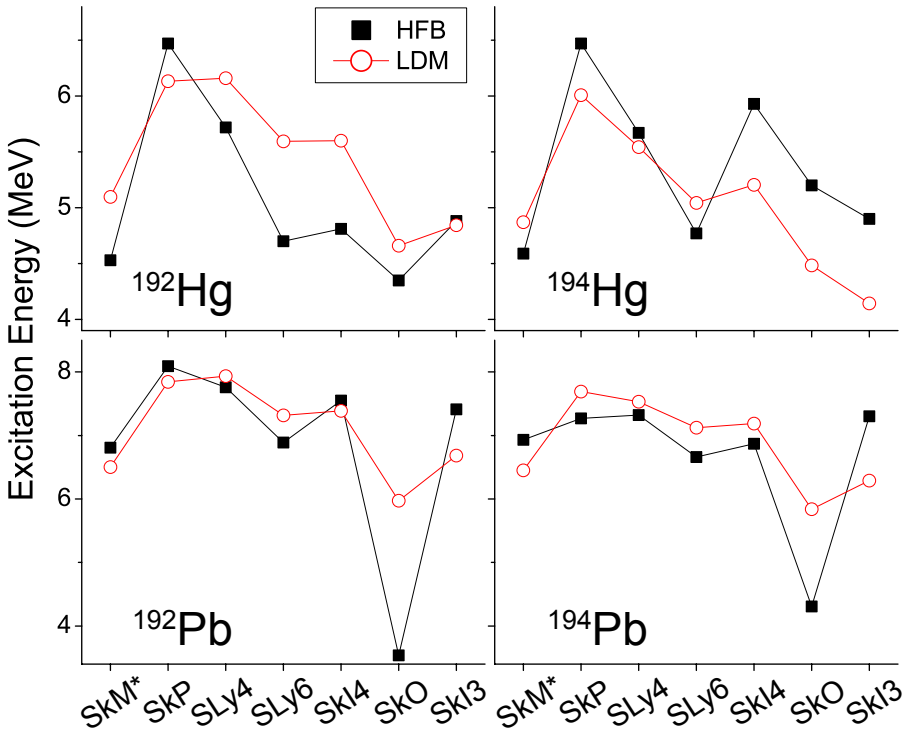

Figure 4.6: (color-online) Same as in Fig. 4.5 except for SD bandheads in ^{192,194}Hg and ^{192,194}Pb.

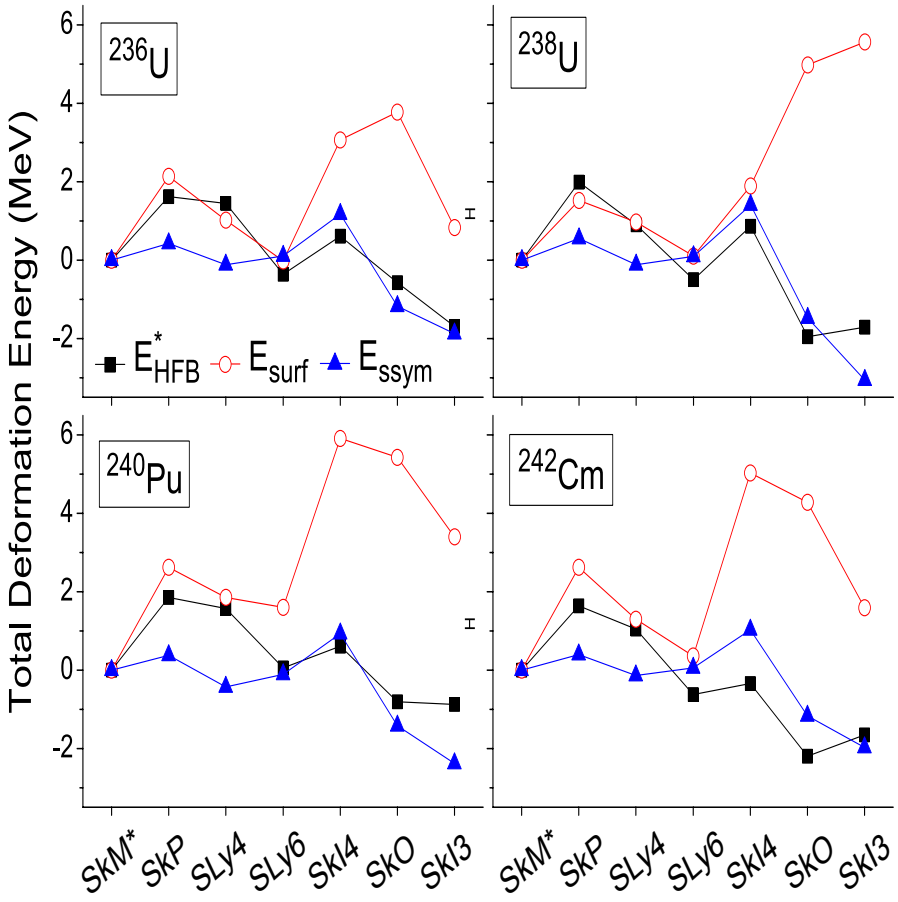

Figure 4.7: (color-online) Surface and surface-symmetry contributions to the LDM excitation energy of fission isomers in the actinides compared to the smooth HFB excitation energy for the same Skyrme EDFs as in Figs. 4.5 and 4.6. All curves are shown relative to SkM* results.

state are obtained in HFB.

The LDM results are compared to the smooth HFB energy EHFB. To facilitate interpretation, all curves are normalized to SkM* values. In this way, we can better compare relative variations obtained in various EDFs. It is interesting to see that the inter-EDF fluctuations of $\tilde{E}^*_{HFB}$ are rather well correlated with the surface-symmetry energy. In other words, the contribution from the Coulomb and curvature terms (not plotted in Fig. 4.7 for better legibility) cancel out the surface term to a large extent. This result is significant because it seems to confirm the simple analysis in a realistic case: in nuclei having large neutron excess I (here of the order of I $\approx$ 0.2), differences in deformation energy between various EDF parameterizations reflect the differences of the surface-symmetry coefficient. By contrast, a similar analysis of individual macroscopic contributions in the Hg-Pb region does not allow to pin down a single LDM term as a primary deformation driver.

Chapter 5

Surface symmetry energy and the r-process

An interesting aspect of this project is related to the investigation of fission properties of heavy neutron-rich nuclei that can participate in the astrophysical r-process. The r-process occurs at high-temperatures ($0.01 < T_9 < 10MeV$) and high-density (neutron rich) stellar environment of supernovae [126] or neutron star mergers and is believed to be responsible for synthesis of about half of the elements beyond iron. Above proton number $Z = 80$ r-process can be terminated by fission.

5.1 Excitation energies of fission isomers in neutron rich Uranium isotopes

This section presents the results of calculations for band heands of fission isomers in neutron rich Uranium isotopes. These results nicely illustrate typical behavior expected in heavy fission systems. Figure 5.1 shows the behavior of the neutron Fermi energy vs the neutron number as given by HFB (HFBTHO) large-scale calculations. The plot provides information about the locaion of the neutron drip line and offers an insight about the isotopes participating in the r-process ($\lambda_n \approx 1MeV$). In the following discussion, we consider uranium isotopes from ^{236}U (N=144) to ^{312}U (N=220).

Figure 5.2 shows PESs obtained in HFB calculations for this set of uranium isotopes,

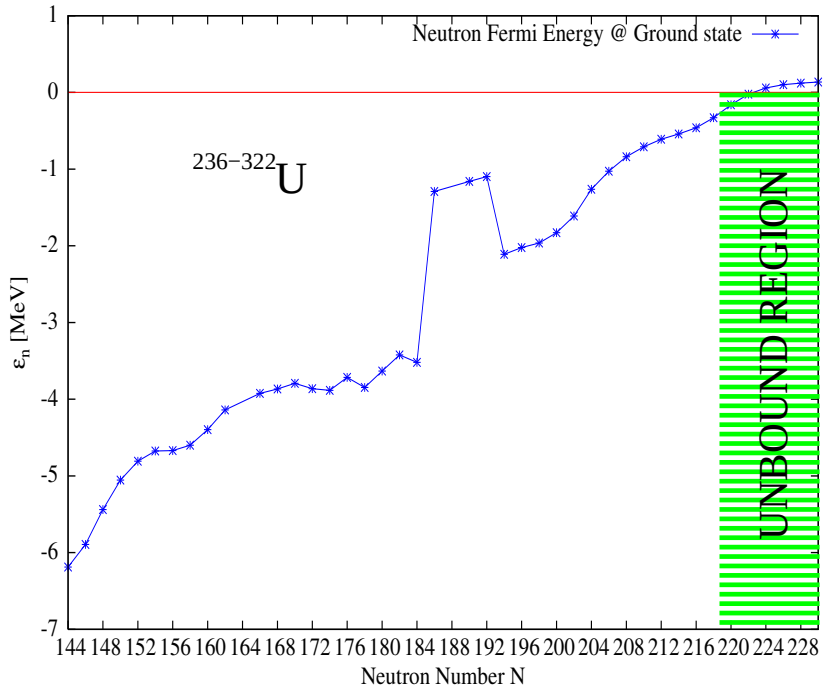

Figure 5.1: Neutron Fermi energy λ_n as function of the neutron number N from unconstrained HFB+SkM* Skyrme calculation for ground states of even-even uranium isotopes. The two-neutron drip line corresponds to $\lambda_n = 0$

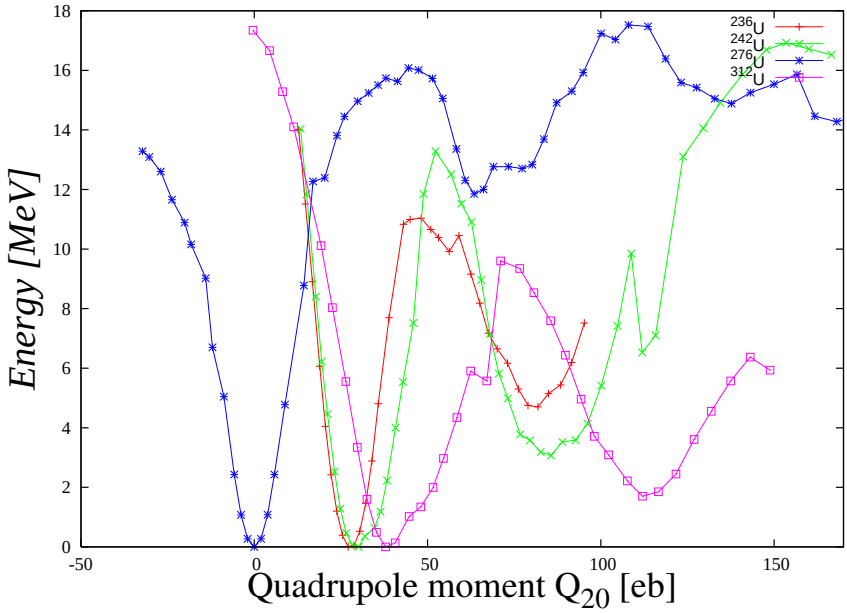

Figure 5.2: Potential Energy Surface from a HFB calculation with a SkM* Skyrme interaction in the case of neutron-rich U nuclei (axial cases only). See details in the text.

starting from ^{236}U. What immediately can be seen is that ground state, fission barrier, and fission isomer change their energy and shape with N. In the case of ^{276}U the barrier and fission isomer have the highest energies due to the magic neutron number $N = 184$. As we approach the dripline neutron rich isotope ^{312}U, the fission barrier and fission isomer become lower in energy, which means increasing instablity against fission. All calculations in Figure 5.2 are done in axial symmetry. That means that the presented fission barriers are only approximate, the inner barriers are strongly affected by the triaxiallity. However, the change in the fission isomer energy demonstrates the evolution of the shell structure with the N. Figure 5.2 offers just a qualitative picture.

Figure 5.3 shows the large-scale trend of the HFB fission isomer excitation energy along the neutron rich Uranium isotopes. The strong increase of the excitation energy between $A = 270$ and 280 is due to the neutron shell $N = 184$. It has been predicted that $N = 184$ is magic [127, 128]. Table 5.1 presents the neutron shell correction for the ground state and the fission isomer in several uranium isotopes. We see that around ^{276}U, the ground state neutron shell correction has a minimum. The presented conclusions are in agreement with the results in [127, 128]. Table 5.1 also demonstrates that the residual neutron shell

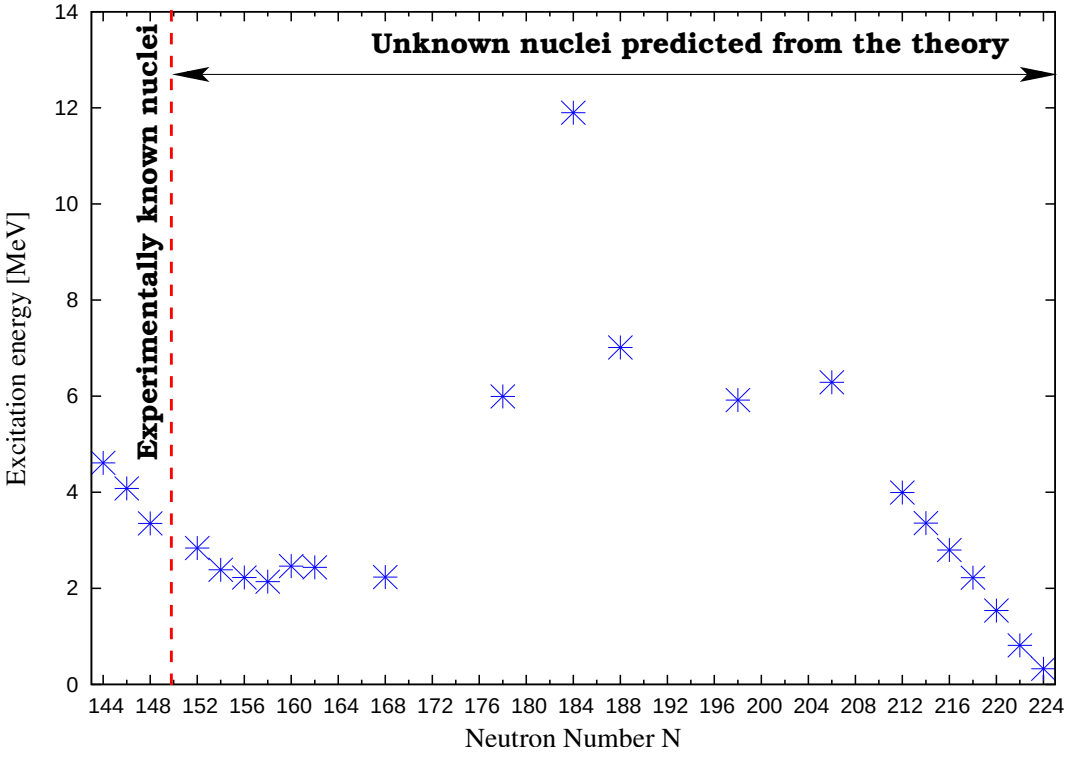

Figure 5.3: Excitation energy of the first fission isomers in neutron-rich Uranium nuclei beyond ^{236}U predicted in HFB+SkM* model.

correction between ground state and fission isomer is close to zero for the most neutron rich uranium isotopes. Therefore, we can conclude that LDM has major contribution to the deformation energy of the very neutron rich systems.

Figure 5.4 gives the relative percentage of the contributions of the terms inside the LDM macroscopic excitation energy based on the realistic HFB deformations in Figure 5.5. What can be seen is that the total sum of surface, surface-symmetry, and curvature energies increase with the neutron number of the isotope. The surface-symmetry energy percentage increases to $\approx 20\%$ in the region around ^{300}U, while in the case of the well-known ^{236}U it is less than 10%. Therefore, the fissility of the heavy neutron-rich Uranium isotopes has to be modified and to include surface-symmetry contribution in addition to the surface and Coulomb energies [72], i.e.

$$\mathrm{x} \equiv \frac{E_{\mathrm{Coul}}(\mathrm{sph})}{2E_{\mathrm{surf}}(\mathrm{sph})} \approx \frac{Z^2}{47A(1-\eta I^2)}, \tag{5.1}$$

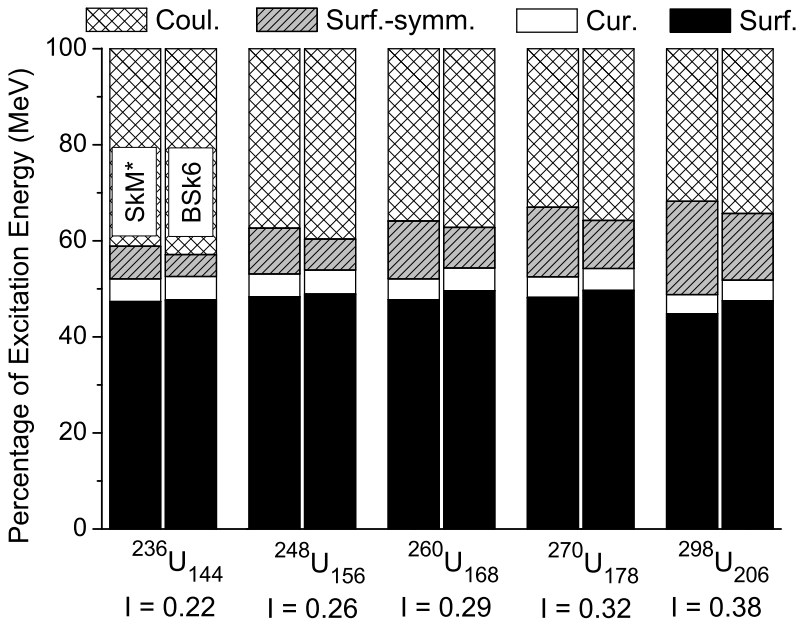

Figure 5.4: Relative contributions of the Coulomb, surface-symmetry, curvature and surface terms to the equivalent LDM deformation energy of SD states in a sequence of U isotopes. Calculations are based on SkM* and BSk6 EDF. Coulomb polarization is included by using the procedure from Chapter 3.

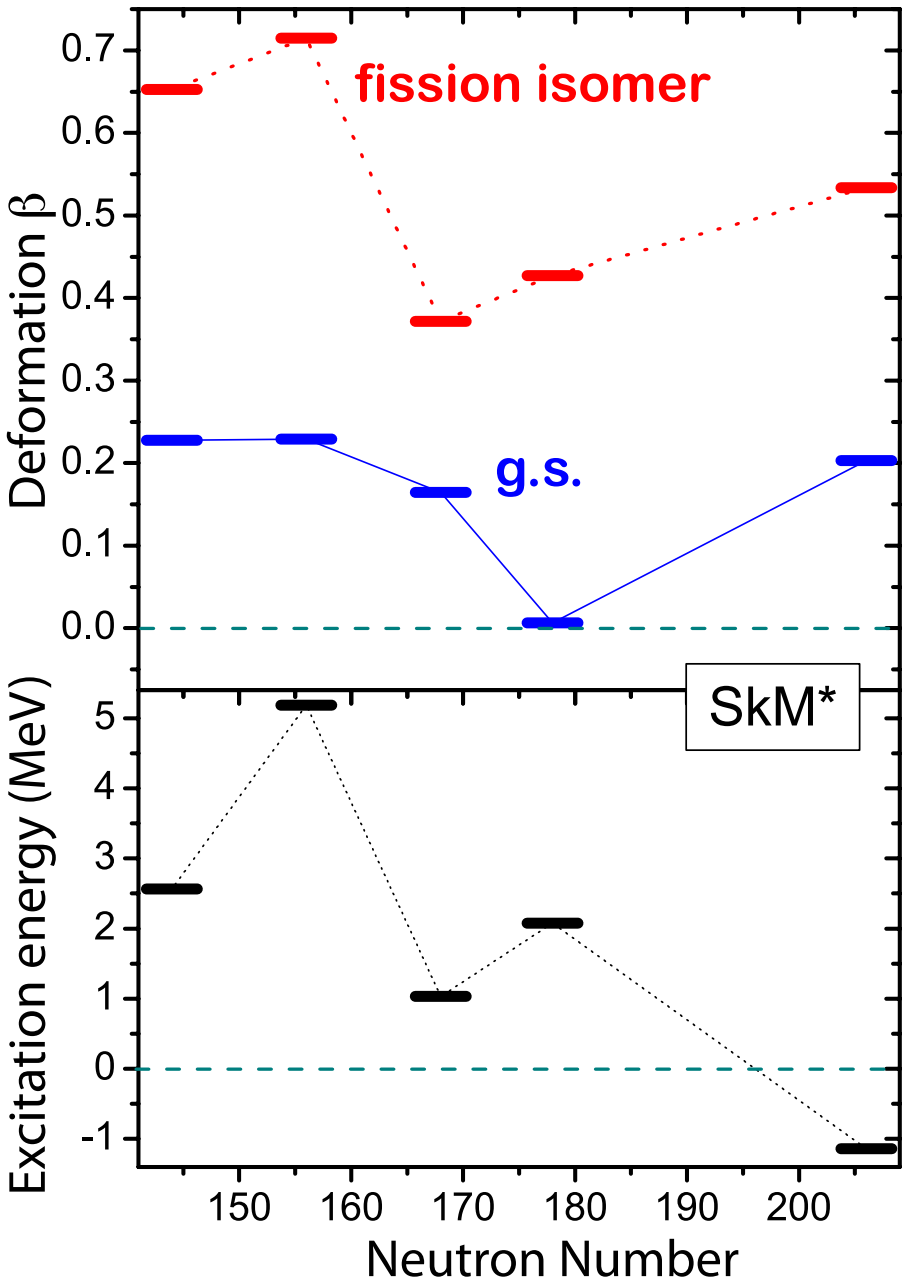

Figure 5.5: Upper panel: Quadrupole deformation β_2 of the ground-state and fission isomer for the same nuclei as in Figure 5.4. Lower panel: LDM excitation energy.

Isotope	δE^{GS}_{shell} [MeV]	$\delta E^{Isomer}_{shell}$ [MeV]
^{236}U	-7.0923	-0.4889
^{260}U	-1.2075	1.7634
^{270}U	-3.1478	0.8901
^{276}U	-7.9736	3.4965
^{280}U	-1.9748	0.2718
^{306}U	-0.6949	1.0088
^{308}U	-0.7326	0.4949
^{310}U	-1.5739	-1.7132
^{312}U	-1.0300	-0.7612

Table 5.1: Neutron shell corrections for the ground state and the fission isomer in few Uranium isotopes with the SkM* interaction. Shell corrections were extracted from CHF calculations (no pairing) in the equilibrium ground state and fission isomer minima. The last are obtained from HFB data shown on Figure 5.3.

where $\eta \equiv \frac{-a_{\rm ssym}}{a_{\rm surf}}$. If $x > 1$, the nuclear liquid drop is unstable against fission. In the presence of neutron excess, the fissility increases, i.e. the fission rate increases. From the data on Table 2.2, it can be seen that η is 1.9 for BSk6, 2.9 for SkM* and 4.16 for SkI3. This means η is model dependent. In [133] $\eta = 1.7826$ was used.

These results are based on calculations with three particular Skyrme forces: SkM*, BSk6 and SkI3. The SkM* EDF has a surface-symmetry coefficient close to average. BSk6 gives a reasonable rms deviation for the excitation energies on Figure 4.4. If we take SkI3, which has a very large surface-symmetry coefficient a_{ssym}, all the conclusions reached can be much different, as shown on Figure 5.6.

Equation (5.4) has another uncertainty related to the constants of LDM (for example the charge radii and the Coulomb polarization within the Coulomb energy $E_{\rm Coul}$). Therefore the value of the constant 47 can change as well, and Figure 5.6 should be taken as qualitative guidance. However, the most important information is that fission rate is governed by the LDM fission barriers due to the vanishing shell effects at high temperature stellar conditions. Here one see the impact of the surface-symmetry energy and its

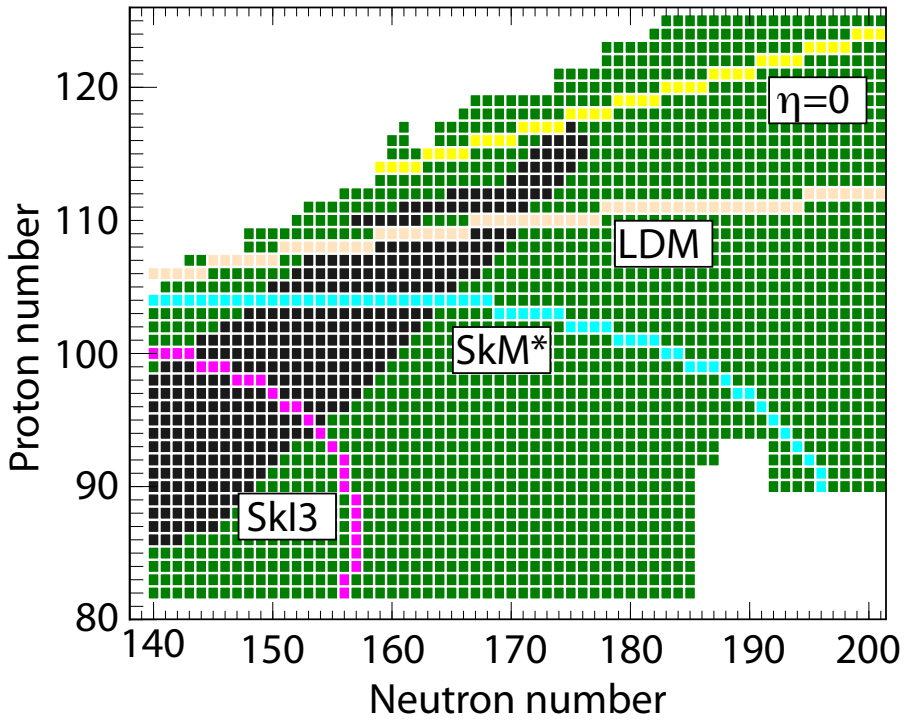

Figure 5.6: The upper part of the chart of nuclides with the $x = 1$ limit indicated for the SkI3 and SkM* EDFs, the value of $\eta = 1.7826$ used in [133] (LDM) and no isospin dependence ($\eta = 0$). The region of known nuclides is marked by black squares.

uncertainty on the level of EDF parametrization.

Chapter 6

Conclusions

This work contains a comprehensive study of deformation properties of nuclear energy density functionals based on the leptodermous expansion of the smooth nuclear energy. Since symmetry and surface-symmetry terms in the expansion are strongly correlated, a way to resolve them is to consider data on deformed neutron-rich nuclei, in which the surface-symmetry term is amplified. Based on intuitive LDM arguments, we argue that deformation properties of neutron-rich nuclear drops are governed by an interplay of the deformation-driving Coulomb and surface-symmetry terms, and the surface energy that acts against shape deformation. To estimate this interplay, we extracted the smooth deformation part of the HFB energy by means of the shell correction procedure. Self-consistent DFT calculations for excitation energies of SD states show marked differences in their predictions depending on the parametrization used. For the set of EDFs considered, the average rms deviation between predicted energies of SD states and experimental values is 1.26 MeV. Within this set, the MSk1 parametrization provides the best overall reproduction of the data: the corresponding rms deviation is 0.53 MeV, and this set a benchmark for future improvements. For the subset of fission isomer data, the best performer is SkI4: its rms deviation is 0.48 MeV.

We showed that inter-parametrization differences reflect to a large extent macroscopic properties of EDFs. In particular, our calculations indicate that the bulk deformation properties of actinides are strongly driven by surface-symmetry effects, while in the proton-rich $A \sim 190$ nuclei there is more competition between the various macroscopic contributions.

This finding should have an impact on the fissility of heavy, very neutron-rich nuclei of the kind encountered e.g. in the r-process.

In this work, two DFT solvers were used: HFODD Ref. [66, 67, 69, 70] and HFBTHO Ref. [68]. Both solvers are based on harmonic oscillator basis expansion technique. The calculated DFT energies depend on the size of the basis. The optimal basis size which provides the best convergence and the lowest theoretical error bar (less than 200 keV) has been determined.

The main code developments carried out here are related to the analysis of the HFB results through the construction of new routines that calculate the proper surface deformations, charge radii, and shell corrections that take into account continuum effects. Surface deformations were needed for the analysis of the HFB results with respect to the LDM. This was done by means of a new routine, SMOMENTS that calculates surface multipole moments from the HFB densities. "SMOMENTS" charge radii were used in the calculations of the Coulomb polarization effects in ^{192,194}Hg, ^{192,194,196}Pb, ^{236,238}U, ^{240}Pu and ^{242}Cm, as well as for neutron rich Uranium isotopes. The analysis of the shell corrections was made by a routine based on the standard Strutinsky's renormalization procedure using the Green function method, which accounts for the s.p. continuum effects ("modified Plateau conditions") Ref. [102] and Ref. [104]. The shell correction analysis is consistent with respect to the previous studies Ref. [55].

The results obtained in this paper suggest that adding to the list of observables data on strongly deformed nuclear states (such as excitation energies of SD states or fission barriers), combined with the usual constraints on bulk properties and shell structure, should constrain quite effectively the surface properties of the nuclear EDF. Such a strategy is currently being pursued within the UNEDF project [91, 92]. On the experimental side, new information on deformed properties on neutron-rich systems is the key.

Bibliography

Bibliography

[1] David Gross and Frank Wilczek, *Phys.Rev.D* **8** *3633 (1973).*

[2] J.Negele and N.Orland, "Quantum Many-Particle Physics", *Frontiers in Physics, Lecture Notes Series, 1988.*

[3] B.D.Day, *Rev.Mod.Phys.* **37** *719 (1967).*

[4] P. Möller, J.R. Nix, W.D. Myers, and W.J. Swiatecki,*Atom. Data and Nucl. Data Tables* **59***, 185 (1995).*

[5] P.Danielewicz, J.Lee, *Nucl. Phys. A* **818***, 36 (2009).*

[6] J.Dobaczewski and W.Nazarewicz, *Phil.Trans.R.Soc.Lond. A* **356***, 2007 (1998).*

[7] J.Dobaczewski and W.Nazarewicz, *Prog. of Theor. Phys. Suppl. No* **146***, 70 (2002).*

[8] J.Erler, P.Klüpfel, P.-G.Reinhard, *J.Phys.G:Nucl.Part.Phys.* **37***, 064001(2010).*

[9] W.D.Myres and W.J.Swiatecki, *Nucl.Phys.* **81** *1 (1966).*

[10] W.D.Myers and W.J.Swiatecki, *Ann.Phys.* **55** *186 (1969).*

[11] W.Satula, R.Wyss, *Phys. Lett. B* **572***, 152 (2003).*

[12] W.Satula, R.Wyss, M.Rafalski *Phys. Rev. C* **74***, 011301 (2006).*

[13] http://massexplorer.org/

[14] M.V. Stoitsov, J. Dobaczewski, W. Nazarewicz, S. Pittel, and D.J. Dean, *Phys. Rev. C* **68***, 054312 (2003).*

[15] S. Goriely, N. Chamel, and J.M. Pearson, *Phys.Rev.Lett.* **102**, *152503 (2009).*

[16] C.Y. Wong, *Ann. Phys. (NY)* **77**, *279 (1973).*

[17] J. Dechargé, J.-F. Berger, M. Girod, and K. Dietrich, *Nucl. Phys. A* **716**, *55 (2003).*

[18] Y.Yu, A. Bulgac, and P. Magierski, *Phys. Rev. Lett.* **84**, *412 (2000).*

[19] W. Nazarewicz, M. Bender, S. Cwiok, P.H. Heenen, A.T. Kruppa, P.-G. Reinhard, and T. Vertse, *Nucl. Phys. A* **701**, *165 (2002).*

[20] F.J.Vinãs, M. Centelles, and M. Warda, *Int. J. Mod. Phys. E* **17**, *177 (2008).*

[21] P. Möller, A.J. Sierk, T. Ichikawa, and A. Iwamoto, *Prog. Theor. Phys. Suppl.* **154**, *21 (2004).*

[22] V. Zagrebaev and W. Greiner, *Phys. Rev. C* **78**, *034610.*

[23] A.G.W. Cameron, *Astrophys. J.* **587**, *327 (2002).*

[24] E. Kolbe, K. Langanke, and G.M. Fuller, *Phys. Rev. C* **92**, *111101 (2004).*

[25] P. Magierski and P.H. Heenen, *Phys. Rev. C* **65**, *045804.*

[26] W.G. Newton and J.R. Stone, *Phys. Rev. C* **79**, *055801.*

[27] W. Nazarewicz, J. Dobaczewski, M. Matev, S. Mizutori, and W. Satula, *Acta Phys. Pol.* **32**, *2349 (2001).*

[28] N. Michel, K. Matsuyanagi, M. Stoitsov, *Phys.Rev.C* **78**, *044319 (2008).*

[29] M.W.Kiron, *Nucl.Phys. A* **798**, *29 (2008).*

[30] A.W.Steiner. M.Prakash, J.M.Lattimer, and P.J.Ellis, *Phys.Rep.* **411**, *325 (2005).*

[31] E.Lippiarini and S.Stringari, *Phys.Lett. B* **112**, *421 (1982).*

[32] T.Mukhopadhyay and D.N.Basu, *Nucl.Phys. A* **789**, *201 (2007).*

[33] N.Wang and M.Liu, *Phys.Rev.C* **81**, *067302 (2010).*

[34] P.Danielewicz, *Nucl.Phys. A* **727**, *233 (2003).*

[35] A.E.L. Diepernik and P.Van Isaacker, *Eur.Phys.J. A* **32**, *11 (2007).*

[36] P.Danielewicz and Jenny Lee, *AIP Conf. Proc.* **947** *301 (2007); arXiv: 0708.2830v1.*

[37] T.D.Lee and C.N.Yang, *Phys.Rev.* **105**, *1119 (1957).*

[38] T.Papenbrock *Phys.Rev.A* **72**, *041603 (2005).*

[39] A.Bhattcharyya, T.Papenbrock *Phys.Rev.A* **74**, *041602 (2006).*

[40] A. Gezerlis and G.F.Bertsch *Phys.Rev.Lett* **105** *212501 (2010).*

[41] M.Brack,J.Damgard,A.S.Jensen, H.C.Pauli, V.M.Strutinsky, and C.Y.Wong, *Rev. Mod. Phys.* **44**, *320 (1972).*

[42] M.Bolsteri, E.O.Fiset, J.R.Nix, J.L.Norton, *Phys.Rev.C* **5**, *1050 (1972).*

[43] A.Bohr and B.R.Mottelson, *Nuclear Structure, Vol. II (W.A.Benjamin, New York, 1975).*

[44] S.G.Nilsson and I.Ragnarsson, *Shapes and Shells in Nuclear Structure (Cambridge University Press, Cambridge, 1995).*

[45] M.Bender,P.-H.Heenen, and P.-G.Reinhard, *Rev. Mod. Rev.* **75**, *121 (2003).*

[46] J.R.Stone, and P.-G.Reinhard, *Prog. Part. and Nucl. Phys.***58**, *587 (2007).*

[47] F.Chappert, M.Girod, and S.Hilaire, *Phys. Lett. B* **668**, *420 (2008).*

[48] P.Klüpfel, P.-G.Reinhard, T.J.Bürvenich, and J.A.Maruhn, *Phys.Rev.C* **79**, *034310 (2009).*

[49] S.Goriely, N.Chamel, and J.M.Pearson, *Phys.Rev.C* **82**, *035804 (2010).*

[50] S.K.Bogner, R.J.Furnstahl, and A.Schwenk *Prog.Part.Nuclear Phys.***45** *243 (2000).*

[51] J. Dobaczewski, W. Nazarewicz, and T.R. Werner, *Physica Scripta T* **56**, *15 (1995).*

[52] J. Dobaczewski, W. Nazarewicz, and M.V. Stoitsov, *Eur. Phys. J. A* **15**, *21 (2002).*

[53] B.Gebermariam, T.Duguet, and S.K.Bogner, *Phys. Rev. C* **82** *014305 (2010).*

[54] William D. Myers and W.J.Swiatecki, *Ann.Phys.* **55**, *395 (1969).*

[55] P.-G. Reinhard, M. Bender, W. Nazarewicz, and T. Vertse *Phys. Rev. C* **73**, *014309 (2006).*

[56] P.Hohenberg and W. Kohn, *Phys.Rev. 136, B***864** *(1964).*

[57] J.Dechargé and D.Gogny *Phys. Rev. C* **21**, *1568 (1980).*

[58] M.N.Kirson, *Nucl. Phys. A* **258**, *29 (2008).*

[59] E.Lipparini and S.Stringari, *Phys.Lett. B* **112**, *421 (1982).*

[60] V.M.Kolomietz and A.I.Sanzhur, *Phys.Rev.C* **81**, *024324 (2009).*

[61] E.Perlinska et al, *Phys.Rev.C* **69**, *014316 (2004).*

[62] A.N.Andreyev, M.Huyse, P.Van Duppen, et al. *Nature Vol.***405**, *430 (2000).*

[63] M.J.A de Voigt, J.Dudek,. and Z. Szymanski, *Rev.Mod.Phys.* **55**, *949 (1983).*

[64] S.Bjornholm and J.E.Lynn, *Rev.Mod.Phys.* **52**, *725 (1980).*

[65] S.Mizutori, J. Dobaczewski, G.A.Lalazissis, W. Nazarewicz, P.-G. Reinhard, *Phys. Rev. C* **61**, *044326 (2000).*

[66] J. Dobaczewski, and J. Dudek, *Comput.Phys.Commun.* **102** *166 (1997).*

[67] J. Dobaczewski, and P.Olbratowski, *Comput.Phys.Commun.* **158** *158 (2004).*

[68] M.V.Stoitsov, J. Dobaczewski, W. Nazarewicz, P.Ring *Comput.Phys.Commun.* **167** *43 (2005).*

[69] J. Dobaczewski, and P.Olbratowski, *Comput.Phys.Commun.* **167** *214 (2005).*

[70] J. Dobaczewski, W.Satula, B.G.Carlsson, J.Engel, P.Olbratowski, M.Sadziak, et al, *Comput.Phys.Commun.* **167** *214 (2005).*

[71] M.V.Stoitsov, J. Dobaczewski, P.Ring, and S.Pittel, *Phys.Rev. C* **61**, *034311 (2000).*

[72] P.Ring and P.Schuck, *The Nuclear Many Body Problem, Springer-Verlag, Berlin, 1980.*

[73] R.Bengtsson, J.Dudek, W. Nazarewicz, and P. Olanders, *Phys.Scr.* **39**, *196 (1989).*

[74] R. W. Hasse, *Ann.Phys.* **68** *(1971) 377.*

[75] M.Farine, J.M.Pearson, and B.Rouben, *Nucl.Phys. A* **304**, *317 (1978).*

[76] M.Farine, M.Côte, and J.M.Pearson, *Nucl.Phys. A* **338**, *86 (1980).*

[77] M.Farine, M.Côte, and J.M.Pearson, *Phys.Rev. C* **24**, *303 (1981).*

[78] F.Tondeur et al, *Nucl.Phys.A* **420**, *297(1984).*

[79] Skalski, Private communication

[80] B.Pomorska, K.Pomorski, *Z.Phys.A* **348**, *169 (1994).*

[81] M.Kleban, B. Nerlo-Pomorska, J.-F.Berger, J. Dechargeé, M.Girod, and S.Hilarie, *Phys.Rev.C* **65**, *024309 (2002).*

[82] B. Nerlo-Pomorska and K.Mazurek, *Phys.Rev.C* **66**, *064305 (2002).*

[83] G.A.Lalazissis, J.König, and P.Ring, *Phys.Rev.C* **55**, *540 (1997).*

[84] J. Dobaczewski, W. Nazarewicz, T.R.Werner, *Z.Phys.A* **354**, *27 (1996).*

[85] J.C.Pei, M.V.Stoitsov, G.I.Fann, W. Nazarewicz, N.Schunck, F.R.Xu, *Phys. Rev. C* **78**, *064306 (2008).*

[86] B.K.Jennings et al., *Nucl.Phys. A253, 29, (1975).*

[87] P.Maris, J.P.Vary, and A.M.Shirokov, *Phys. Rev. C* **79**, *014308 (2009).*

[88] G.Hagen, D.J.Dean, M.Hjorth-Jensen, T.Papenbrock, and A.Schwenk, *Phys. Rev. C* **76**, *044305 (2007).*

[89] A.Staszczak, M.Stoitsov, A.Baran, and W.Nazarewicz, *Eur.Phys.J.A* **46**, *85 (2010).*

[90] W.Younes and D.Gogny, *Phys.Rev.C* **80**, *054313, (2009).*

[91] M.Kortelainen, T.Lesinski, J.Moré, W.Nazarewicz, J.Sarich, N.Schunck, M.V.Stoitsov, and S.Wild *Phys.Rev.C* **82**, *024313 (2010).*

[92] M.Kortelainen, R.J.Furnstahl, W.W.Nazarewicz, and M.V.Stoitsov, *Phys.Rev.C* **82**, *011304, (2010).*

[93] M.Brack and P.Quentin, *Phys. Lett.* **B56**, *421 (1975).*

[94] B.M.Nyakó, J.R.Cresswell, P.D.Forsyth, D.Howe, P.J.Nolan, M.A.Riley, J.F.Sharpey-Schafer, J.Simpson, N.J.Ward, and P.J.Twin *Phys.Rev.Lett.* **52** *(1984).*

[95] V.M.Strutinski, *Nucl.Phys. A* **95**, *420 (1967).*

[96] V.M.Strutinski, *Nucl.Phys. A* **122**, *1 (1968).*

[97] H. Flocard et al., *Nucl.Phys.A, Vol.***203**, *Issue 3, 433,1973.*

[98] L.Bennour, P-H.Heenen, P.Bonche, J. Dobaczewski, and H.Folcard, *Phys. Rev. C* **40**, *2834 (1989).*

[99] B.A.Brown, *Phys. Rev. C* **58**, *220 (1998).*

[100] F.L.Braghin, D. Vautherin, and A.Abada, *Phys. Rev. C* **52**, *2504 (1995).*

[101] F.Tondeur, S.Goriely, J.M.Pearson, and M.Onsi, *Phys. Rev. C* **62**, *024308 (2000).*

[102] A.T.Kruppa, M.Bender, W.Nazarewicz, P.-G.Reinhard, T.Vertse, and S.Ćwiok, *Phys.Rev.C* **61**, *034313 (2000).*

[103] P.Salamon, A.T.Kruppa, T.Vertse, *Phys.Rev.C* **81**, *064322 (2010)*

[104] T. Vertse, A.T. Kruppa and W. Nazarewicz, *Phys. Rev. C* **61**, *064317 (2000).*

[105] S.Ćwiok, W.Dudek, P.Kaszýnski, W.Nazarewicz, *Eur.Phys.J. A* **23**, *387 (2005).*

[106] J. Bartel, P. Quentin, M. Brack, C. Guet, and H.B. Håkansson *Nucl. Phys. A* **386**, *79 (1982).*

[107] J. Dobaczewski, H. Flocard and J. Treiner, *Nucl. Phys. A* **422**, *103 (1984).*

[108] M. Samyn, S. Goriely, P.-H. Heenen, J.M. Pearson, and F. Tondeur, *Nucl. Phys. A* **700**, *142 (2002).*

[109] S. Goriely, M. Samyn, M. Bender, and J.M. Pearson, *Phys. Rev. C* **68**, *054325 (2003).*

[110] E. Chabanat, P. Bonche, P. Haensel, J. Meyer, and R. Schaeffer, *Nucl. Phys. A* **635**, *231 (1998).*

[111] P.-G. Reinhard and H. Flocard, *Nucl. Phys. A,* **584**, *467 (1995).*

[112] P.-G. Reinhard, D.J. Dean, W. Nazarewicz, J. Dobaczewski, J.A. Maruhn, and M.R. Strayer, *Phys. Rev. C* **60**, *014316 (1999).*

[113] P.-G. Reinhard, M. Rufa, J. Maruhn, W. Greiner, and J. Friedrich, *Z. Phys. A* **323**, *13 (1986).*

[114] M. Rufa, P.-G. Reinhard, J. A. Maruhn, W. Greiner, and M. R. Strayer, *Phys. Rev. C* **38**, *390 (1988).*

[115] M. Bender, K. Rutz, P.-G. Reinhard, J.A. Maruhn, and W. Greiner, *Phys. Rev. C* **60**, *034304 (1999).*

[116] K. Pomorski and J. Dudek, *Phys. Rev. C* **67**, *044316 (2003).*

[117] unedf.org/

[118] B. Singh, R. Zywina, R.B. Firestone, *Nucl. Data Sheets* **97**, *241 (2002).*

[119] E.A. Henry *et al*, *Z. Phys. A* **338**, *469 (1991); Phys. Rev. C* **49**, *2849 (1994).*

[120] R.G. Henry *et al*, *Phys. Rev. Lett.* **73**, *777 (1994).*

[121] A. Lopez-Martens, *et al*, *Phys. Rev. Lett.* **77**, *1707 (1996).*

[122] K. Hauschild *et al*, *Phys. Rev. C* **55**, *2819 (1997).*

[123] A.N. Wilson, G.D. Dracoulis, A.P. Byrne, P.M. Davidson, G.J. Lane, R.M. Clark, P. Fallon, A. Görgen, A.O. Macchiavelli, and D. Ward, *Phys. Rev. Lett.* **90**, *142501 (2003).*

[124] A.N. Wilson, *et al*, *Phys. Rev. Lett.* **95**, *182501 (2005).*

[125] J. C. Pei, W. Nazarewicz, J. A. Sheikh, and A. K. Kerman *Phys. Rev. Lett.* **102**, *192501 (2009).*

[126] I.V.Panov, E.Kolbe, B.Pfeiffer, T.Rauscher, K.-L.Kratz, F.-K.Thielemann, *Nucl. Phys. A* **747**, *633 (2005).*

[127] I.V.Panov, I.Yu.Korneev, et al. *Astronomy and Astrophysics* **A61**, *513 (2010).*

[128] S.Goriely, M. Samyn, and J.M.Pearson, *Phys. Rev. C* **75**, *064312 (2007).*

[129] P.-G. Reinhard and W. Nazarewicz, *Phys. Rev. C* **81**, *051303 (2010).*

[130] M. Warda, X. Viñas, X. Roca-Maza, and M. Centelles, *Phys. Rev. C* **80**, *024316 (2009).*

[131] P.-G. Reinhard, *Nucl.Phys.A* **649**, *305c(1999).*

[132] S.Mizutori, J. Dobaczewski, G.A.Lalazissis, W. Nazarewicz, P.-G. Reinhard, *Phys. Rev. C* **61**, *044326 (2000).*

[133] G.I.Bell, *Phys.Rev.* **158**, *1127 (1967).*

[134] N. Nikolov, N. Schunck, W. Nazarewicz, M. Bender, and J. C. Pei, *Phys. Rev. C 83, 034305*

[135] M.Kortelainen, J. McDonnell, J. Moré, W. Nazarewicz, J. Sarich, N. Schunck, M. V. Stoitsov, and S. Wild *in progress.*

Vita

Nikola I. Nikolov was born on May 10, 1979, Sofia, Bulgaria. He graduated with honors from Sofia Technical High School for Chemical and Bio-technologies "Prof. Assen Zlatarov" in May 1998. He continued Physics major in Sofia University "St. Kliment Ohridski" and graduated with master degree in nuclear and particle physics in Spring 2004. He jointed University of Tennessee, Knoxville, and accepted a research assistantship to study surface symmetry energy of nuclear energy density functionals under the supervision of Prof. Witold Nazarewicz.